DTU Library

Silicon as an anisotropic mechanical material
Deflection of thin crystalline plates

Thomsen, Erik Vilain; Reck, Kasper; Skands, Gustav Erik; Bertelsen, Christian Vinther; Hansen, Ole

Document Version
Early version, also known as pre-print

[Link back to DTU Orbit](#)

Silicon as an Anisotropic Mechanical Material: Deflection of Thin Crystalline Plates

Erik V. Thomsen, Kasper Reck, Gustav Skands, Christian Bertelsen and Ole Hansen

Department of Micro- and Nanotechnology, DTU Nanotech, Technical University of Denmark, Building 345E, DK-2800 Lyngby, Denmark

Abstract

While silicon is an anisotropic material it is often in literature treated as an isotropic material when it comes to plate calculations. This leads to considerable errors in the calculated deflection. To overcome this problem, we present an in-depth analysis of the bending behavior of thin crystalline plates. An analysis of the compliance tensor for the 32 different crystal classes shows, that for thin plates, only 5 different types of plates exist. An anisotropic plate equation valid for crystalline thin plates is derived and solved for circular, elliptic, rectangular and square plates using both exact analytical expressions and approximate expressions calculated by the Galerkin method. The results are applied to plates made on silicon (001), (011) and (111) substrates, respectively, and analytical equations for the deflection, strain energy and resonance frequency of such plates are presented. These expressions are in excellent agreement with anisotropic finite element calculations. The calculated deflection differs less than 0.1%, for both circular and rectangular plates, compared to finite element calculations. The results are presented as ready-to-use facilitating accurate analytical models involving crystalline plates, such as those often found in the field of micro electro mechanical systems. The effect of elastic boundary conditions is taken into account by using an effective radius of the plate.

Keywords: Anisotropic plate theory, Micromechanics, Silicon

1. Introduction

Thin plates are important as structural elements in many micro electro mechanical systems (MEMS). They enable devices such as capacitive micromachined ultrasonic transducers (CMUTs) [1], and a range of pressure sensors including piezoresistive [2], capacitive [3, 4] and optical pressure sensors [5]. These devices all use a thin plate which is deflected due to either a pressure or an applied voltage.

In the design of such devices some of the important parameters are the deflection of the plate, the center deflection, the strain energy and the resonance frequency. In some cases these devices use a plate made of an isotropic material, such as amorphous SiO_2, and the static deflection surface, $w(x,y)$, is calculated by solving the Kirchhoff–Love *isotropic plate equation* [6]

$$\frac{\partial^4 w}{\partial x^4} + 2\frac{\partial^4 w}{\partial x^2 \partial y^2} + \frac{\partial^4 w}{\partial y^4} = \frac{p}{D_i} \tag{1}$$

where p is the applied pressure difference across the plate and the isotropic flexural rigidity, D_i, is given by

$$D_i = \frac{E}{12(1-\nu^2)}h^3 \tag{2}$$

where E is the Young's modulus, ν is the Poisson's ratio, and h is the thickness of the plate. The plate equation is then solved using appropriate boundary conditions and the obtained deflection surface can be used to calculate the

stress and strain distributions, important for piezoresistive sensors, or in the case of CMUTs and capacitive pressure sensors the capacitance of the device can be found. This procedure works well if the plate material is isotropic and for circular and elliptic plates an exact solution is available [6].

Expressed in cylindrical coordinates, the static deflection $w(r)$ for a thin circular plate with radius, a, clamped at the periphery is [6]

$$w(r) = w_0 \left[1 - \left(\frac{r}{a}\right)^2\right]^2 \tag{3}$$

assuming that the boundary conditions are given by $\partial w(0)/\partial r = 0$, $\partial w(a)/\partial r = 0$, $w(a) = 0$ and that the center deflection, $w(0)$, is finite. The center deflection is given by

$$w_0 = w(0) = \frac{pa^4}{64D_i}. \tag{4}$$

These expressions are only valid, when the deflection of the plate is sufficiently small compared to the plate thickness, i.e. for $h/w_0 \gtrsim 5$, such that stress stiffening effects can be ignored. Also, it is assumed, that the aspect ratio of the plate is sufficiently large, $a/h \gtrsim 40$, which ensures that the plate is thin enough that the contribution from shear deformation is small. In the calculations it is assumed that the plate is clamped ($\partial w(a)/\partial r = 0$, $w(a) = 0$) at the boundary. Real plates, however, have elastic boundaries [7, 8] and the effect of this is to make the plate more soft.

This effect can be captured analytically by introducing an effective radius as explained in Appendix A.

For rectangular and square plates a simple exact solution to the plate differential equation does not exist. Instead, approximate solutions based on series expansions are normally used [6, 9, 10].

The center deflection, w_{0i}, of a clamped square isotropic plate, having sidelength $2L$, exposed to a uniform load, p, is given by [9]

$$w_{0i} = 0.020245105392 \frac{L^4 p}{D_i}. \tag{5}$$

The prefactor in this equation has recently been calculated with high precision using the classical double cosine series expansion to the deflection [9].

The plate material, however, is not always isotropic. Many devices use plates of crystalline silicon fabricated either by bulk micromachining [11, 12] or wafer bonding techniques [13–16]. Crystalline silicon is an anisotropic material with a diamond cubic crystal structure widely used as a mechanical material [17]. Plates made on silicon (111) substrates behave like isotropic plates, with constant Young's modulus and Poisson's ratio and the isotropic plate equation can then be used to calculate the deflection of such plates. However, for other silicon substrates, such as silicon (001) and silicon (011), Young's modulus and Poisson's ratio are strongly anisotropic[18], and (1) and (2) therefore cannot be used to calculate the deflection. Despite of this fact, these equations are widely used in research papers and textbooks (for example [19–22]), using for example mean or effective values of the Young's modulus and the Poisson's ratio [23], perhaps due to the absence of a good alternative. This can result in errors up to 10-25% in the calculated center deflections. The problem is illustrated in Fig. 1 that shows a cross section ($y = 0$) of the deflection surface of a thin clamped circular plate made on a silicon (001) substrate as calculated by finite element modeling (FEM) taking anisotropy into account. The two dashed curves show the deflection as calculated from (3) and (4) using values of Young's modulus and Poisson's ratio corresponding to the [100] and [110] directions on the silicon substrate, respectively. These solutions to the *isotropic* plate equation are clearly not a satisfactory approximation to the *anisotropic* problem as the difference in the calculated center deflections are 8-10% compared to the exact anisotropic solution. Using mean values of the Poisson's ratio and Young's modulus reduces the difference in the calculated center deflections to around 1% but is still an unsatisfactory approach. For beams and cantilevers the solution is to use the Young's modulus and Poisson's ratio corresponding to the orientation of the structure. However, for plates this procedure cannot be applied.

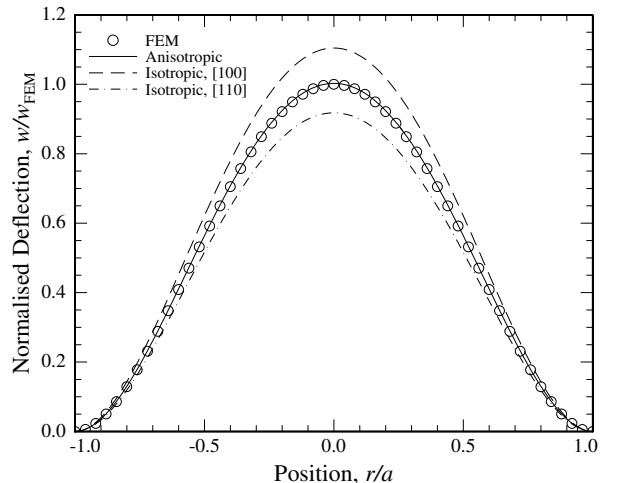The solution to this problem is to use the proper

Figure 1: Cross section of the deflection surface ($y = 0$) for a circular plate on a silicon (001) substrate. The results from a FEM calculation taking the anisotropic nature of silicon into account are plotted using the symbols. The dashed and dot-dashed curves, corresponds to the isotropic result, (3) and (4) using values of the Poisson's ratio and Young's modulus corresponding to the [100] and [110] directions on the (001) silicon substrate, respectively. The deflections are normalized with respect to center deflection obtained with FEM. The full line corresponds to the exact analytical result for the anisotropic plate, to be derived in section 9, as expressed by (3) and (31). The isotropic approach clearly leads to large errors in the center deflection (difference compared to FEM is around 10%) whereas the analytical anisotropic result is in excellent agreement, difference in calculated center deflection is less than 0.1%, with the FEM calculation.

anisotropic *generalized plate equation* [24, 25]

$$\frac{\partial^4 w}{\partial x^4} + k_1 \frac{\partial^4 w}{\partial x^3 \partial y} + k_2 \frac{\partial^4 w}{\partial x^2 \partial y^2} + k_3 \frac{\partial^4 w}{\partial x \partial y^3} + k_4 \frac{\partial^4 w}{\partial y^4} = \frac{p}{D_a}. \tag{6}$$

The plate equation coefficients k_1 to k_4 and the anisotropic flexural rigidity, D_a, to be defined later, depend on the elastic constants of the plate material. This plate equation has been used extensively in the field of solid mechanics [25] to study the deflection of laminates. However, the expression for the plate equation coefficients in the equation were derived assuming that the plate is monoclinic. To overcome this restriction (which for example excludes the correct treatment of Si(111) plates), we will derive the plate equation for an *arbitrary* crystal class.

In an anisotropic material the elastic constants depend on the orientation of the plate with respect to the crystallographic coordinate system. The procedure to solve the plate equation is therefore 1) to obtain the elastic constants *for the plate*, 2) to calculate the parameters in the anisotropic plate equation and finally 3) to solve the differential equation using suitable boundary conditions for the plate in question.

This approach will be used to find center deflections, strain energy, resonance frequency and deflection surfaces for plates fabricated on (001), (011) and (111) silicon substrates. The results will allow designers to easily perform

calculations on silicon plates and the results will be shown to be in excellent agreement, difference in center deflection of less than 0.1% as shown in Fig. 1, with anisotropic finite element calculations.

The article is organized as follows: The definitions of stress, strain and the transformation of the stiffness and compliance tensors are described in sections 2 and 3 and the anisotropic plate equation is derived in section 4. Section 5 is devoted to calculation of the strain energy and the resonance frequency of plates. Then, in sections 6 and 7 the anisotropic plate equation is solved for a number of different plate geometries (circular, elliptic, square and rectangular plates) using exact solutions for the circular and elliptic plates and applying the Galerkin method for square and rectangular plates. This yields simple expressions for the center deflections, and the deflection of the plates are in excellent agreement with FEM. The focus is then shifted towards silicon as an *anisotropic mechanical material* . First, the mechanical properties of silicon substrates are described in section 8. Then, the anisotropic plate theory is used to study the anisotropic behavior of thin circular, section 9, and square, section 10, plates made on (001), (011) and (111) silicon substrates, respectively. Section 11 provides an example on how to use the derived theory on circular and square silicon plates and provides simple, yet accurate, ready to use expressions for several important plate design parameters. Finally, in section 12, the article ends with conclusions.

2. Stress and strain

The states of stress and strain in a linear elastic material with arbitrary crystal symmetry are fully specified by symmetric second order stress and strain tensors [26]. The linear relation between the stress and strain tensors is described by fourth order compliance or stiffness tensors. In equilibrium the stress and strain tensors in general have six independent elements each, due to the symmetry, and thus the states of stress and strain are conveniently represented, using the 6-vector Voigt notation, as the vectors [27]

$$\boldsymbol{\sigma}^{\mathrm{c}} = \left(\sigma_{xx}^{\mathrm{c}}, \sigma_{yy}^{\mathrm{c}}, \sigma_{zz}^{\mathrm{c}}, \sigma_{yz}^{\mathrm{c}}, \sigma_{xz}^{\mathrm{c}}, \sigma_{xy}^{\mathrm{c}} \right)^T$$
$$= \left(\sigma_1^{\mathrm{c}}, \sigma_2^{\mathrm{c}}, \sigma_3^{\mathrm{c}}, \sigma_4^{\mathrm{c}}, \sigma_5^{\mathrm{c}}, \sigma_6^{\mathrm{c}} \right)^T$$

and

$$\boldsymbol{\varepsilon}^{\mathrm{c}} = \left(\varepsilon_{xx}^{\mathrm{c}}, \varepsilon_{yy}^{\mathrm{c}}, \varepsilon_{zz}^{\mathrm{c}}, 2\varepsilon_{yz}^{\mathrm{c}}, 2\varepsilon_{xz}^{\mathrm{c}}, 2\varepsilon_{xy}^{\mathrm{c}} \right)^T$$
$$= \left(\varepsilon_1^{\mathrm{c}}, \varepsilon_2^{\mathrm{c}}, \varepsilon_3^{\mathrm{c}}, \varepsilon_4^{\mathrm{c}}, \varepsilon_5^{\mathrm{c}}, \varepsilon_6^{\mathrm{c}} \right)^T .$$

Here the superscript c denotes that the value or expression is given in the crystallographic coordinate system and the superscript T denotes the transpose (used for a more compact notation). The elements σ_{pq}^{c} and $\varepsilon_{pq}^{\mathrm{c}}$, $p, q \in [x, y, z]$, are the original tensor elements, while σ_i^{c} and $\varepsilon_i^{\mathrm{c}}$, $i \in [1 \ldots 6]$, are the stress and *engineering* strain

elements that uses a factor of two on the shear strains and therefore the 6-vector engineering strain elements $\varepsilon_i^{\mathrm{c}}$ do not form a tensor.

In 6-vector notation, the compliance and stiffness tensors may conveniently be represented by symmetric matrices (which are not tensors) each with at most 21 independent elements. The compliance tensor for a crystal with a minimum of symmetry elements (triclinic crystal system) is thus represented by the symmetric matrix $\mathbf{s}^{\mathrm{c}}$ [27]

$$\mathbf{s}^{\mathrm{c}} = \begin{pmatrix} s_{11}^{\mathrm{c}} & s_{12}^{\mathrm{c}} & s_{13}^{\mathrm{c}} & s_{14}^{\mathrm{c}} & s_{15}^{\mathrm{c}} & s_{16}^{\mathrm{c}} \\ s_{12}^{\mathrm{c}} & s_{22}^{\mathrm{c}} & s_{23}^{\mathrm{c}} & s_{24}^{\mathrm{c}} & s_{25}^{\mathrm{c}} & s_{26}^{\mathrm{c}} \\ s_{13}^{\mathrm{c}} & s_{23}^{\mathrm{c}} & s_{33}^{\mathrm{c}} & s_{34}^{\mathrm{c}} & s_{35}^{\mathrm{c}} & s_{36}^{\mathrm{c}} \\ s_{14}^{\mathrm{c}} & s_{24}^{\mathrm{c}} & s_{34}^{\mathrm{c}} & s_{44}^{\mathrm{c}} & s_{45}^{\mathrm{c}} & s_{46}^{\mathrm{c}} \\ s_{15}^{\mathrm{c}} & s_{25}^{\mathrm{c}} & s_{35}^{\mathrm{c}} & s_{45}^{\mathrm{c}} & s_{55}^{\mathrm{c}} & s_{56}^{\mathrm{c}} \\ s_{16}^{\mathrm{c}} & s_{26}^{\mathrm{c}} & s_{36}^{\mathrm{c}} & s_{46}^{\mathrm{c}} & s_{56}^{\mathrm{c}} & s_{66}^{\mathrm{c}} \end{pmatrix} . \quad (7)$$

The stiffness matrix $\mathbf{c}^{\mathrm{c}} = (\mathbf{s}^{\mathrm{c}})^{-1}$ has the same topology. Using the stiffness and compliance matrices the linear relations between stress and strain may be written in compact form as the matrix relations [26]

$$\boldsymbol{\sigma}^{\mathrm{c}} = \mathbf{c}^{\mathrm{c}} \boldsymbol{\varepsilon}^{\mathrm{c}}, \text{ and } \boldsymbol{\varepsilon}^{\mathrm{c}} = \mathbf{s}^{\mathrm{c}} \boldsymbol{\sigma}^{\mathrm{c}}. \quad (8)$$

3. Transformation of the stiffness and compliance tensors

Calculations on mechanical structures fabricated in a crystalline material are complicated by the fact that several coordinate systems must be used. The crystalline material itself has a natural coordinate system which is called the crystallographic coordinate system. The mechanical structures are fabricated on substrates cut from the original crystal having some predefined orientation and for the substrates a suitable coordinate system has to be defined. Finally, for the mechanical structures, such as a plate, the coordinate system is most often chosen to be aligned to the structure in a convenient manner, for example along the edges of a rectangular plate, as illustrated in Fig. 2. This means that the plate coordinate system is rotated an angle ψ with respect to the chosen coordinate system of the substrate.

In general, the elements of the stiffness and compliance matrices for the plate depend on the orientation of the plate coordinate system with respect to the crystallographic coordinate system. Thus, these matrices must be calculated *in the plate coordinate system* in order to solve the plate equation. In the following, a superscript c will be used to denote quantities expressed in the crystallographic coordinate system, whereas terms without this subscript are in the plate coordinate system. As an example, the stiffness matrix elements in the crystallographic coordinate system are denoted c_{ij}^{c} whereas the stiffness matrix elements in the plate coordinate system are denoted c_{ij}.

The Cartesian crystal coordinate system has the set of orthonormal base vectors $\hat{\mathbf{e}}_1^{\mathrm{c}}$, $\hat{\mathbf{e}}_2^{\mathrm{c}}$, and $\hat{\mathbf{e}}_3^{\mathrm{c}}$, while the plate coordinate system has the orthonormal base vectors $\hat{\mathbf{e}}_1$,
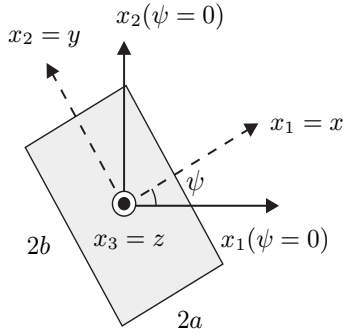
Figure 2: The figure shows the substrate (full line) and plate (dashed line), coordinate systems used in the calculations. The coordinate system for a plate is generally rotated an angle ψ with respect to the main coordinate system for the substrate. The figure also shows a rectangular plate having sidelengths of $2a$ and $2b$ in the x- and y-directions, respectively. The plate is clamped at the periphery as indicated by the thin solid line around the plate. The z-axis is normal to the plane of the plate.

$\hat{\mathbf{e}}_2$, and $\hat{\mathbf{e}}_3$, obtained from the original set of base vectors by three sequential counterclockwise rotations using the Euler angles (ϕ, θ, ψ) in the x-convention as outlined in the Appendix Appendix B. In the x-convention [26] the first rotation (ϕ) is done around the third axis, the second (θ) around the new first axis, and the final (ψ) around the new third axis. Coordinates x_n of a point or a fixed vector in the rotated coordinate system are obtained from the coordinates x_m^c in the original coordinate system using a rotation matrix $\boldsymbol{a}$ with the elements

$$a_{nm} = \hat{\mathbf{e}}_n \cdot \hat{\mathbf{e}}_m^c \qquad (9)$$

i.e. $x_n = \sum_m a_{nm} x_m^c$ with $m, n \in [1, 2, 3]$.

3.1. Stiffness and compliance

The elements of the stress tensor in the crystal and plate coordinate systems, σ_{ml}^c and σ_{nk}, respectively, are related by [27]

$$\sigma_{nk} = \sum_m \sum_l a_{nm} a_{kl} \sigma_{ml}^c \qquad (10)$$

with $k, l, m, n \in [1, 2, 3]$. It follows that a stress transformation matrix $\boldsymbol{\alpha}$ may be defined [26] such that six-vector stresses σ_j^c and σ_i in the crystal and plate coordinate systems, respectively, are related by

$$\sigma_i = \sum_j \alpha_{ij} \sigma_j^c \qquad (11)$$

where $i, j \in [1 \ldots 6]$. The use of the stress transformation matrix $\boldsymbol{\alpha}$ facilitates calculation of the compliance and stiffness matrices $\boldsymbol{s}$ and $\boldsymbol{c}$ in the plate coordinate system, since (a superscript -1 denotes the inverse matrix)[26]

$$\boldsymbol{c} = \boldsymbol{\alpha} \boldsymbol{c}^c \boldsymbol{\alpha}^T, \qquad (12)$$

$$\boldsymbol{s} = (\boldsymbol{\alpha}^T)^{-1} \boldsymbol{s}^c \boldsymbol{\alpha}^{-1}. \qquad (13)$$

Explicitly, the stress transformation matrix $\boldsymbol{\alpha}$ is obtained as

$$\boldsymbol{\alpha} = \left(\begin{array}{ccc} a_{11}^2 & a_{12}^2 & a_{13}^2 \\ a_{21}^2 & a_{22}^2 & a_{23}^2 \\ a_{31}^2 & a_{32}^2 & a_{33}^2 \\ a_{21}a_{31} & a_{22}a_{32} & a_{23}a_{33} \\ a_{31}a_{11} & a_{32}a_{12} & a_{33}a_{13} \\ a_{11}a_{21} & a_{12}a_{22} & a_{13}a_{23} \end{array}\right.$$
$$\begin{array}{ccc} 2a_{12}a_{13} & 2a_{13}a_{11} & 2a_{11}a_{12} \\ 2a_{22}a_{23} & 2a_{23}a_{21} & 2a_{21}a_{22} \\ 2a_{32}a_{33} & 2a_{33}a_{31} & 2a_{31}a_{32} \\ a_{22}a_{33} + a_{23}a_{32} & a_{21}a_{33} + a_{23}a_{31} & a_{22}a_{31} + a_{21}a_{32} \\ a_{12}a_{33} + a_{13}a_{32} & a_{13}a_{31} + a_{11}a_{33} & a_{11}a_{32} + a_{12}a_{31} \\ a_{12}a_{23} + a_{13}a_{22} & a_{13}a_{21} + a_{11}a_{23} & a_{11}a_{22} + a_{12}a_{21} \end{array}\left.\right).$$
$$(14)$$

Thus, knowing the rotation matrix, (9), relating the two coordinate systems, the stiffness and compliance matrix elements in the rotated coordinate system can be found.

3.2. Plane stress

When a structure, such as a plate, is thin compared to its lateral dimensions all stresses related to the $z-$direction are small and may be set to zero (this is the so-called plane stress condition), i.e. $\sigma_3 = \sigma_4 = \sigma_5 = 0$, while the stresses σ_1, σ_2, and σ_6 are non-zero as are in general all the components of strain. Since stresses and strains are linearly related, three linearly independent strain components are sufficient to fully specify the three non-zero stresses. As a result we may, without loss of generality, write

$$\left(\begin{array}{c} \varepsilon_1 \\ \varepsilon_2 \\ \varepsilon_6 \end{array}\right) = \left(\begin{array}{ccc} s_{11} & s_{12} & s_{16} \\ s_{12} & s_{22} & s_{26} \\ s_{16} & s_{26} & s_{66} \end{array}\right) \left(\begin{array}{c} \sigma_1 \\ \sigma_2 \\ \sigma_6 \end{array}\right) \qquad (15)$$

$$= \mathbf{S}_{\text{eff}} \left(\begin{array}{c} \sigma_1 \\ \sigma_2 \\ \sigma_6 \end{array}\right). \qquad (16)$$

The effective compliance matrix $\mathbf{S}_{\text{eff}}$ can always be inverted to form an effective stiffness matrix, $\mathbf{C}_{\text{eff}} = (\mathbf{S}_{\text{eff}})^{-1}$, and thus (15) may be solved for the stresses

$$\left(\begin{array}{c} \sigma_1 \\ \sigma_2 \\ \sigma_6 \end{array}\right) = \left(\begin{array}{ccc} s_{11} & s_{12} & s_{16} \\ s_{12} & s_{22} & s_{26} \\ s_{16} & s_{26} & s_{66} \end{array}\right)^{-1} \left(\begin{array}{c} \varepsilon_1 \\ \varepsilon_2 \\ \varepsilon_6 \end{array}\right) \qquad (17)$$

$$= \left(\begin{array}{ccc} C_{11}^{\text{eff}} & C_{12}^{\text{eff}} & C_{13}^{\text{eff}} \\ C_{12}^{\text{eff}} & C_{22}^{\text{eff}} & C_{23}^{\text{eff}} \\ C_{13}^{\text{eff}} & C_{23}^{\text{eff}} & C_{33}^{\text{eff}} \end{array}\right) \left(\begin{array}{c} \varepsilon_1 \\ \varepsilon_2 \\ \varepsilon_6 \end{array}\right). \qquad (18)$$

Notice, that while the elements of the (3×3) reduced compliance matrix, (15), are obtained directly from the (6×6) compliance matrix, (7), for the plate the reduced stiffness matrix must be found by inverting $\mathbf{S}_{\text{eff}}$.

The effective compliance matrices for the 32 crystal classes are listed in Tab. 1. It is noted, that under the plane

stress condition, only 5 different types of plates, Type I to Type V, exist when grouped according to the effective compliance. It is also noted, that trigonal and hexagonal crystal plates will behave as isotropic plates.

4. Anisotropic plate equation

In this section we derive a general plate equation valid for thin plates of a material with arbitrary crystal symmetry. The calculations are performed in a Cartesian coordinate system with the z-axis normal to the plane of the plate. The plates are assumed to be stress free before the differential pressure load is applied.

The starting point is the force balance in the $z-$direction for a thin plate with the thickness h and the pressure load p

$$-p = \int_{-h/2}^{h/2} z \left(\frac{\partial^2 \sigma_1}{\partial x^2} + 2\frac{\partial^2 \sigma_6}{\partial x \partial y} + \frac{\partial^2 \sigma_2}{\partial y^2} \right) \mathrm{d}z \qquad (19)$$

which results from combining force and moment balances for the plate. Notice the sign convention used for the pressure: A positive value of p will lead to a positive deflection in the $z-$direction.

On kinematic grounds, the strains in the small deflection approximation are [28]

$$\varepsilon_1 = -z\frac{\partial^2 w}{\partial x^2}, \ \varepsilon_2 = -z\frac{\partial^2 w}{\partial y^2}, \text{ and } \varepsilon_6 = -2z\frac{\partial^2 w}{\partial x \partial y} \qquad (20)$$

where $w = w(x,y)$ is the deflection of the neutral plane in the $z-$direction. Inserting (17) and (20) in (19) results in the *generalized plate equation*

$$\frac{\partial^4 w}{\partial x^4} + k_1\frac{\partial^4 w}{\partial x^3 \partial y} + k_2\frac{\partial^4 w}{\partial x^2 \partial y^2} + k_3\frac{\partial^4 w}{\partial x \partial y^3} + k_4\frac{\partial^4 w}{\partial y^4} = \frac{p}{D_\mathrm{a}} \qquad (21)$$

where we have defined the *generalized flexural rigidity*, D_a, as

$$\frac{12}{h^3}D_\mathrm{a} = C_{11}^{\mathrm{eff}}$$

$$= \frac{s_{26}^2 - s_{22}s_{66}}{s_{16}^2 s_{22} - 2s_{12}s_{16}s_{26} + s_{12}^2 s_{66} + s_{11}\left(s_{26}^2 - s_{22}s_{66}\right)} \qquad (22)$$

and the *generalized plate equation coefficients*

$$k_1 = 4\frac{C_{13}^{\mathrm{eff}}}{C_{11}^{\mathrm{eff}}} = 4\frac{s_{16}s_{22} - s_{12}s_{26}}{s_{26}^2 - s_{22}s_{66}} \qquad (23)$$

$$k_2 = 2\frac{\left(C_{12}^{\mathrm{eff}} + 2C_{33}^{\mathrm{eff}}\right)}{C_{11}^{\mathrm{eff}}}$$

$$= 2\frac{2s_{11}s_{22} + s_{16}s_{26} - s_{12}\left(2s_{12} + s_{66}\right)}{s_{22}s_{66} - s_{26}^2} \qquad (24)$$

$$k_3 = 4\frac{C_{23}^{\mathrm{eff}}}{C_{11}^{\mathrm{eff}}} = 4\frac{s_{12}s_{16} - s_{11}s_{26}}{s_{22}s_{66} - s_{26}^2} \qquad (25)$$

$$k_4 = \frac{C_{22}^{\mathrm{eff}}}{C_{11}^{\mathrm{eff}}} = \frac{s_{16}^2 - s_{11}s_{66}}{s_{26}^2 - s_{22}s_{66}}. \qquad (26)$$

Type	$12D_\mathrm{a}/h^3$
V	$\dfrac{s_{26}^2 - s_{22}s_{66}}{s_{16}^2 s_{22} - 2s_{12}s_{16}s_{26} + s_{12}^2 s_{66} + s_{11}\left(s_{26}^2 - s_{22}s_{66}\right)}$
IV	$\dfrac{s_{16}^2 - s_{22}s_{66}}{s_{16}^2(s_{11} + 2s_{12} + s_{22}) + \left(s_{12}^2 - s_{11}s_{22}\right)s_{66}}$
III	$\dfrac{s_{22}}{s_{11}s_{22} - s_{12}^2}$
II	$\dfrac{s_{11}}{s_{11}^2 - s_{12}^2}$
I	$\dfrac{s_{11}}{s_{11}^2 - s_{12}^2}$

Table 2: Expressions for the anisotropic flexural rigidity, (22). The plate types are the same as in Tab. 1.

The plate equation (21) with the coefficients (22)–(26) is valid for plates of arbitrary crystal class as long as the plates are sufficiently thin and the deflection sufficiently small as described in the introduction.

Tab. 2 shows the expressions for the flexural rigidities and Tab. 3 shows the plate equation coefficients for the five different types of plates. Plates of Type V are highly anisotropic. For plates of Type IV it is found that $k_1 = -k_3$. It is noted, that $k_1 = k_3 = 0$ for plates of Type I, II and III and in these cases, the generalized plate equation, (21), reduces to the *reduced plate equation*

$$\frac{\partial^4 w}{\partial x^4} + k_2\frac{\partial^4 w}{\partial x^2 \partial y^2} + k_4\frac{\partial^4 w}{\partial y^4} = \frac{p}{D_\mathrm{a}}. \qquad (27)$$

This equation does not depend on k_1 and k_3 and is identical in form with the orthotropic plate equation [6] the plate equation coefficients, however, are different. This reduced plate equation is also valid, if the symmetry of the plate deflection satisfies the condition $\partial^4 w/\partial x^3 \partial y = \partial^4 w/\partial y^3 \partial x = 0$, which is the case for a circular plate. Finally, we note, that the reduced plate equation is identical to the isotropic plate equation, (1), when the plate is of Type I.

5. Strain energy and resonance frequency

Once the anisotropic plate equation has been solved, the strain energy can be calculated from the deflection, $w(x,y)$. In the case of plane stress, the strain energy, W, stored in an elastic anisotropic body is given by [29]

$$W = \frac{1}{2}\iiint_V \left(\sigma_1\varepsilon_1 + \sigma_2\varepsilon_2 + \sigma_6\varepsilon_6\right) \mathrm{d}x\,\mathrm{d}y\,\mathrm{d}z \qquad (28)$$

where V denotes that the integral is performed over the entire volume of the elastic body. The strains can be evaluated using (20) and the stresses calculated using (17). When the strain energy is known, the resonance frequency of a plate, ω, can be estimated using the Rayleigh-Ritz method [10]

$$\omega^2 = \frac{2W}{\iint_A h\rho w(x,y)^2 \mathrm{d}x\,\mathrm{d}y} \qquad (29)$$

where A denotes that the integral is performed over the area of the plate and ρ is the density of the plate. This

5

Type	Class	Effective compliance, S_{eff}.	Effective stiffness, C_{eff}.
V	Triclinic Monoclinic (e.g., Si(011) sub.)	$\begin{pmatrix} s_{11} & s_{12} & s_{16} \\ s_{12} & s_{22} & s_{26} \\ s_{16} & s_{26} & s_{66} \end{pmatrix}$	$\begin{pmatrix} s_{11} & s_{12} & s_{16} \\ s_{12} & s_{22} & s_{26} \\ s_{16} & s_{26} & s_{66} \end{pmatrix}^{-1}$
IV	Tetragonal (Classes 4,-4,4/m) (e.g., Si(001) sub.)	$\begin{pmatrix} s_{11} & s_{12} & s_{16} \\ s_{12} & s_{22} & -s_{16} \\ s_{16} & -s_{16} & s_{66} \end{pmatrix}$	$\begin{pmatrix} s_{11} & s_{12} & s_{16} \\ s_{12} & s_{22} & -s_{16} \\ s_{16} & -s_{16} & s_{66} \end{pmatrix}^{-1}$
III	Orthotropic Tetragonal (Classes 4mm, -42m,422,4/mmm)	$\begin{pmatrix} s_{11} & s_{12} & 0 \\ s_{12} & s_{22} & 0 \\ 0 & 0 & s_{66} \end{pmatrix}$	$\begin{pmatrix} -\frac{s_{22}}{s_{12}^2-s_{11}s_{22}} & \frac{s_{12}}{s_{12}^2-s_{11}s_{22}} & 0 \\ \frac{s_{12}}{s_{12}^2-s_{11}s_{22}} & -\frac{s_{11}}{s_{12}^2-s_{11}s_{22}} & 0 \\ 0 & 0 & \frac{1}{s_{66}} \end{pmatrix}$
II	Cubic	$\begin{pmatrix} s_{11} & s_{12} & 0 \\ s_{12} & s_{11} & 0 \\ 0 & 0 & s_{44} \end{pmatrix}$	$\begin{pmatrix} \frac{s_{11}}{s_{11}^2-s_{12}^2} & -\frac{s_{12}}{s_{11}^2-s_{12}^2} & 0 \\ -\frac{s_{12}}{s_{11}^2-s_{12}^2} & \frac{s_{11}}{s_{11}^2-s_{12}^2} & 0 \\ 0 & 0 & \frac{1}{s_{44}} \end{pmatrix}$
I	Isotropic Trigonal Hexagonal (e.g., Si(111) sub.)	$\begin{pmatrix} s_{11} & s_{12} & 0 \\ s_{12} & s_{11} & 0 \\ 0 & 0 & 2\left(s_{11}-s_{12}\right) \end{pmatrix}$	$\begin{pmatrix} \frac{s_{11}}{s_{11}^2-s_{12}^2} & -\frac{s_{12}}{s_{11}^2-s_{12}^2} & 0 \\ -\frac{s_{12}}{s_{11}^2-s_{12}^2} & \frac{s_{11}}{s_{11}^2-s_{12}^2} & 0 \\ 0 & 0 & \frac{1}{2s_{11}-2s_{12}} \end{pmatrix}$

Table 1: Effective compliance and stiffness matrices for the different crystal classes. When the condition of plane stress applies, only five different types of plates exist. For plates of Type IV and V, the inversion of the effective compliance matrix yields results that are too lengthy to fit in the table, and therefore the expressions for the effective stiffness is not given for these types of plates.

Type	k_1	k_2	k_3	k_4
V	$\frac{4(s_{16}s_{22}-s_{12}s_{26})}{s_{26}^2-s_{22}s_{66}}$	$\frac{4s_{11}s_{22}+2s_{16}s_{26}-2s_{12}(2s_{12}+s_{66})}{s_{22}s_{66}-s_{26}^2}$	$\frac{4(s_{12}s_{16}-s_{11}s_{26})}{s_{22}s_{66}-s_{26}^2}$	$\frac{s_{16}^2-s_{11}s_{66}}{s_{26}^2-s_{22}s_{66}}$
IV	$\frac{4s_{16}(s_{12}+s_{22})}{s_{16}^2-s_{22}s_{66}}$	$\frac{2\left(s_{16}^2-2s_{11}s_{22}+s_{12}(2s_{12}+s_{66})\right)}{s_{16}^2-s_{22}s_{66}}$	$-k_1$	$\frac{s_{16}^2-s_{11}s_{66}}{s_{16}^2-s_{22}s_{66}}$
III	0	$\frac{4s_{11}s_{22}-2s_{12}(2s_{12}+s_{66})}{s_{22}s_{66}}$	0	$\frac{s_{11}}{s_{22}}$
II	0	$\frac{4s_{11}^2-2s_{12}(2s_{12}+s_{44})}{s_{11}s_{44}}$	0	1
I	0	2	0	1

Table 3: Plate equation coefficients for the anisotropic plate equation. The plate types are the same as in Tab. 1.

expression yields values close to the exact resonance frequency with deviations of only of 1% being typical.

6. Circular and elliptic plates

The anisotropic plate equation was solved for circular and elliptic plates both analytically and using FEM. For these plates, an exact solution to the generalized plate equation, (21), is available.

6.1. FEM

Finite element simulations were used to investigate the behavior of anisotropic plates and to validate the analytical expressions obtained. The simulations were performed in COMSOL Multiphysics version 4.2a using the small deflection assumption. The FEM simulation results for the center deflection of an isotropic circular plate were compared to the exact analytical solution, (4), and the mesh was optimized to ensure convergence of the simulation. The boundary condition used for the edge of the plates is that the displacements are zero in all directions.

The analytical solution, (4), assumes, that shear deformations can be ignored because the plate is thin. This condition is only met when the aspect ratio of the plate is sufficiently high. Fig. 3 compares the difference between the calculated center deflection using FEM and the analytical result , (4), as function of the aspect ratio of the plate. For aspect ratios larger than 100 an excellent agreement between the two results is seen (difference less than 0.01%), and this aspect ratio was chosen for all FEM calculations in this article.

When the effect of shear deformation on the deflection is taken into account, the exact deflection of a circular isotropic plate is given by [30]

$$w = \frac{pa^4}{64D_i} \left(\left[1 - \left(\frac{r}{a} \right)^2 \right]^2 + \frac{4}{1-\nu} \left(\frac{h}{a} \right)^2 \left[1 - \left(\frac{r}{a} \right)^2 \right] \right) \tag{30}$$

where the second term includes the effect of shear deformation which is proportional to $(h/a)^2$. This term will vanish when the thickness of the plate is small compared to the lateral dimension. The boundary condition used for deriving this equation is that $\partial U/\partial z = 0$ at $z = 0, r = a$ where U is the radial displacement at any point. This equation is shown as the dash-dotted line in Fig. 3. The model predicts the same trend as seen by FEM and the small difference between the two results is due to the use of slightly different boundary conditions. For an aspect ratio of 20, the center deflection differs around 1% from the analytical result for pure bending.

6.2. Analytical solution

For circular and elliptic plates an exact solution to the anisotropic plate equation can be found. As noted by Illing [31] the shape of the static deflection surface of an anisotropic circular plate is the same as that of an isotropic
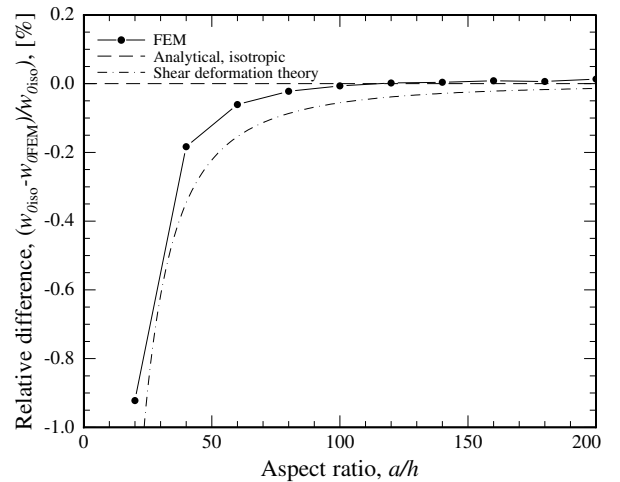

Figure 3: FEM simulation results for the center deflection of an isotropic circular plate were compared to the exact analytical solutions, (4) and (30). The figure compares the difference, shown by the solid circles, between the FEM calculated center deflection and the analytical result, (4), as function of the aspect ratio, a/h, of the plate. The error is on the order of 1% for an aspect ratio of 20. For aspect ratios larger than 100 an excellent agreement between the two results is seen, and this aspect ratio was chosen for the calculations. The dash-dotted line is a plot of (30) which takes shear deformation into account.

plate, however, the effective value of the center deflection is different. By inserting (3) into (21) and solving for the center deflection it is found that

$$w_0 = \frac{a^4 p}{8 \left(3 + k_2 + 3k_4 \right) D_{\mathrm{a}}}. \tag{31}$$

As discussed above, due to the symmetry of the deflection, this equation does not contain k_1 and k_3. If the plate material is isotropic then $D_{\mathrm{a}} = D_{\mathrm{i}}$, $k_2 = 2$ and $k_4 = 1$ and (31) reduces to the well known result expressed in (4). Comparing (31) and (4) it is clear, that one can define an effective flexural rigidity, D_{eff}, as

$$D_{\mathrm{eff}} = \frac{3 + k_2 + 3k_4}{8} D_{\mathrm{a}}. \tag{32}$$

Using this effective flexural rigidity allows to easily change models, such as the lumped element models used for CMUTs [32], based on the deflection of an isotropic circular plate into models for an anisotropic plate just by replacing D_{i} by D_{eff} [33].

Elliptic plates, with major and minor axis of a and b, are treated in a similar manner and the deflection is described by

$$w(x,y) = w_0 \left(1 - \frac{x^2}{a^2} - \frac{y^2}{b^2} \right)^2 \tag{33}$$

where

$$w_0 = \frac{a^4 b^2 p}{8 \left(a^2 k_2 + 3b^2 \left(1 + k_4 \right) \right) D_{\mathrm{a}}}. \tag{34}$$

7

Notice, that the values of the plate equation coefficients and the flexural rigidity needs to be calculated in a coordinate system aligned to the major and minor axis of the elliptic plate.

The strain energy is easily calculated directly from (28) by evaluating the integrals involved using (17) and (20). For a circular anisotropic plate, the result is

$$W = \frac{32\pi w_0^2}{3a^2}\frac{3 + k_2 + 3k_4}{8}D_\mathrm{a} = \frac{32\pi w_0^2}{3a^2}D_\mathrm{eff} \tag{35}$$

$$= \frac{\pi a^6 p^2}{48 D_\mathrm{a}(k_2 + 3k_4 + 3)} \tag{36}$$

which is the same result as for an isotropic plate where D_i enters the equation instead of D_eff. The resonance frequency of the anisotropic circular plate is calculated using (29)

$$\omega^2 = \frac{320}{3a^4 h\rho}\frac{3 + k_2 + 3k_4}{8}D_\mathrm{a} = \frac{320}{3a^4 h\rho}D_\mathrm{eff}. \tag{37}$$

7. Rectangular and square plates

For rectangular and square plates approximate methods have to be used in order to calculate the deflection. In this section we will use the Galerkin method [10] to find approximate analytical expressions for the deflection of rectangular and square plates for any of the five different types of plates.

The Galerkin method has been used by Mbakogu and Pavlovic [34] to study bending of clamped orthotropic plates. The orthotropic plate equation has the same the form as the reduced generalized plate equation, (27). Therefore, the results for the orthotropic plate is directly applicable to plates of Type I–III with suitable substitution of the plate equation coefficients. For plates of Type IV and V (i.e. tetragonal, monoclinic and triclinic anisotropic plates), where the generalized plate equation (21), has to be solved, the procedure used by [34] was extended to solve the anisotropic plate equation for an *arbitrary* plate type.

7.1. The Galerkin method

Based on the generalized anisotropic plate equation, (21), we define the operator $\mathbf{H}$ as

$$\mathbf{H} = \frac{\partial^4}{\partial x^4} + k_1\frac{\partial^4}{\partial x^3 \partial y} + k_2\frac{\partial^4}{\partial x^2 \partial y^2} + k_3\frac{\partial^4}{\partial x \partial y^3} + k_4\frac{\partial^4}{\partial y^4} \tag{38}$$

such that the anisotropic plate equation can be written as

$$\mathbf{H}w - p/D_\mathrm{a} = 0. \tag{39}$$

The deflection surface is approximated by the series [34]

$$w(x,y) = \sum_{k=0,1,\ldots}^{k_m}\sum_{l=0,1,\ldots}^{l_m}\lambda_{kl}\phi_{kl}(x,y) \tag{40}$$

where $k_m = k_l$ is the maximum summation index. The Galerkin system of equations is build as [10, 34]

$$\iint_A \phi_{00}\left(\mathbf{H}w - \frac{p}{D_\mathrm{a}}\right)\mathrm{d}x\,\mathrm{d}y = 0$$

$$\iint_A \phi_{01}\left(\mathbf{H}w - \frac{p}{D_\mathrm{a}}\right)\mathrm{d}x\,\mathrm{d}y = 0$$

$$\vdots$$

$$\iint_A \phi_{k_m l_m}\left(\mathbf{H}w - \frac{p}{D_\mathrm{a}}\right)\mathrm{d}x\,\mathrm{d}y = 0. \tag{41}$$

The deflection, $w(x,y)$, is then found by substituting (40) into (41) and solving the resulting linear equation system to find the coefficients λ_{kl}. This calculation was performed using the symbolic mathematical programme Mathematica 9.0.

7.2. Deflection

We now consider a rectangular plate with sidelengths of $2a$ and $2b$, $b \geq a$, clamped along the edges as shown in Fig. 2. We assume that [34]

$$\phi_{kl}(x,y) = \left(x^2 - a^2\right)^2\left(y^2 - b^2\right)^2 x^k y^l \tag{42}$$

such that the trial deflection function is given by

$$w \approx \left(x^2 - a^2\right)^2\left(y^2 - b^2\right)^2\sum_{k=0,1,\ldots}^{k_m}\sum_{l=0,1,\ldots}^{l_m}\lambda_{kl}x^k y^l. \tag{43}$$

This expression satisfies the clamped boundary conditions, and the center deflection, w_0, is given by

$$w_0 = w(0,0) = \lambda_{00}a^4 b^4. \tag{44}$$

We now consider three different trial functions

$$\begin{aligned} 1)\ w^\mathrm{m} &= \lambda_{00}^\mathrm{m}\phi_{00} \\ &= \left(x^2 - a^2\right)^2\left(y^2 - b^2\right)^2\lambda_{00}^\mathrm{m} \end{aligned} \tag{45}$$

$$\begin{aligned} 2)\ w^\mathrm{n} &= \lambda_{00}^\mathrm{n}\phi_{00} + \lambda_{20}^\mathrm{n}\phi_{20} + \lambda_{02}^\mathrm{n}\phi_{02} \\ &= \left(x^2 - a^2\right)^2\left(y^2 - b^2\right)^2\left(\lambda_{00}^\mathrm{n} + \lambda_{20}^\mathrm{n}x^2 + \lambda_{02}^\mathrm{n}y^2\right) \end{aligned} \tag{46}$$

$$\begin{aligned} 3)\ w^\mathrm{o} &= \lambda_{00}^\mathrm{o}\phi_{00} + \lambda_{11}^\mathrm{o}\phi_{11} + \lambda_{20}^\mathrm{o}\phi_{20} + \lambda_{02}^\mathrm{o}\phi_{02} \\ &= \left(x^2 - a^2\right)^2\left(y^2 - b^2\right)^2 \\ &\quad \times \left(\lambda_{00}^\mathrm{o} + \lambda_{11}^\mathrm{o}xy + \lambda_{20}^\mathrm{o}x^2 + \lambda_{02}^\mathrm{o}y^2\right) \end{aligned} \tag{47}$$

having one, three and four terms selected from the expansion (43), respectively. The first two trial functions, w^m and w^n, have only even terms in x and y and they therefore lead to expressions containing only k_2 and k_4 and not k_1 and k_3. The reason for this is, that the terms in the plate equation containing k_1 and k_3 involves $\partial^4 w/\partial x^3 \partial y$ and $\partial^4 w/\partial y^3 \partial x$. When these derivatives are applied to even functions in x and y the result is an uneven function which will vanish when the integrals in (41) are performed. Such

trial functions are therefore only useful when $k_1 = k_3 = 0$, i.e. for plates of Type I–III.

The trial function w^{o} contains the uneven term xy which ensures that even terms in x and y containing k_1 and k_3 will appear in the integrand. Therefore, the trial function w^{o} will lead to expressions containing all plate equation coefficients and as such allows for *any* of the five different plate types. We now consider the results obtained using these trial functions.

7.2.1. One term

The most simple approach is to use only one term in the expansion (43). Using the test function w^{m}, (45), and performing the procedure described above it is found that

$$\lambda_{00}^{\mathrm{m}} = \frac{49}{128\left(7b^4 + 2a^2b^2k_2 + 7a^4k_4\right)}\frac{p}{D_{\mathrm{a}}} \qquad (48)$$

and the center deflection, $w_0^{\mathrm{m}} = w^{\mathrm{m}}(0,0)$, is

$$w_0^{\mathrm{m}} = \frac{49a^4b^4}{128\left(7b^4 + 2a^2b^2k_2 + 7a^4k_4\right)}\frac{p}{D_{\mathrm{a}}} \qquad (49)$$

which for a square plate, $a = b = L$, reduces to

$$w_{0\mathrm{sq}}^{\mathrm{m}} = \frac{49}{128\left(7 + 2k_2 + 7k_4\right)}\frac{L^4 p}{D_{\mathrm{a}}}. \qquad (50)$$

7.2.2. Three terms (Plate types I, II and III)

We now use the three term test function w^{n}, (46), and perform the procedure described above. The calculated expressions of $\lambda_{00}^{\mathrm{n}}$, $\lambda_{20}^{\mathrm{n}}$ and $\lambda_{02}^{\mathrm{n}}$ are shown in Tab. 4. The center deflection, w_0^{n}, is

$$w_0^{\mathrm{n}} = \lambda_{00}^{\mathrm{n}} a^4 b^4. \qquad (51)$$

The deflection normalized to the center deflection, $w^{\mathrm{n}}/w_0^{\mathrm{n}}$, can be written as

$$\frac{w^{\mathrm{n}}}{w_0^{\mathrm{n}}} = \left[1 - \left(\frac{x}{a}\right)^2\right]^2 \left[1 - \left(\frac{y}{b}\right)^2\right]^2$$
$$\times \left[1 + \beta^{\mathrm{n}}\left(\frac{x}{a}\right)^2 + \gamma^{\mathrm{n}}\left(\frac{y}{b}\right)^2\right] \qquad (52)$$

where the *plate deflection parameters* are given by

$$\beta^{\mathrm{n}} = \frac{\lambda_{20}^{\mathrm{n}}}{\lambda_{00}^{\mathrm{n}}}a^2 \quad \gamma^{\mathrm{n}} = \frac{\lambda_{02}^{\mathrm{n}}}{\lambda_{00}^{\mathrm{n}}}b^2. \qquad (53)$$

The plate deflection parameters, β^{n} and γ^{n}, are listed in Tab. 4 and they depend only on the aspect ratio, $c = b/a$, of the plate and the plate equation coefficients k_2 and k_4. It is noted, that $\beta^{\mathrm{n}} = \gamma^{\mathrm{n}}$ when $k_4 = c^4$ which is the case for an isotropic square plate. Expressions for the center deflections are given in Tab. 5.

7.2.3. Four terms (Plate types IV and V)

Finally, we use the four term test function w^{o}, (47), and perform the Galerkin procedure. The calculated values of $\lambda_{00}^{\mathrm{n}}$, $\lambda_{20}^{\mathrm{n}}$, $\lambda_{02}^{\mathrm{n}}$ and $\lambda_{11}^{\mathrm{o}}$ are given in Appendix Appendix C. The center deflection is

$$w_0^{\mathrm{o}} = \lambda_{00}^{\mathrm{o}} a^4 b^4. \qquad (54)$$

The relative deflection, $w^{\mathrm{o}}/w_0^{\mathrm{o}}$, is given by

$$\frac{w^{\mathrm{o}}}{w_0^{\mathrm{o}}} = \left[1 - \left(\frac{x}{a}\right)^2\right]^2 \left[1 - \left(\frac{y}{b}\right)^2\right]^2$$
$$\times \left[1 + \delta^{\mathrm{o}}\left(\frac{x}{a}\frac{y}{b}\right) + \beta^{\mathrm{o}}\left(\frac{x}{a}\right)^2 + \gamma^{\mathrm{o}}\left(\frac{y}{b}\right)^2\right] \qquad (55)$$

where the plate deflection parameters are defined as

$$\beta^{\mathrm{o}} = \frac{\lambda_{20}^{\mathrm{o}}}{\lambda_{00}^{\mathrm{o}}}a^2 \quad \gamma^{\mathrm{o}} = \frac{\lambda_{02}^{\mathrm{o}}}{\lambda_{00}^{\mathrm{o}}}b^2 \quad \delta^{\mathrm{o}} = \frac{\lambda_{11}^{\mathrm{o}}}{\lambda_{00}^{\mathrm{o}}}ab \ . \qquad (56)$$

These can be calculated using the expressions in Appendix Appendix C.

7.3. Strain and stress

The three strains (ε_1, ε_2 and ε_6) for a plate of Type V can be calculated directly from (20) and the expression for the deflection given by (55). The value of the strains at the center of the edges of the plate are important for applications such as piezoresistive pressure sensors. They are given by

$$\varepsilon_1(x = a, \ y = 0) = -\frac{8z\left(1 + \beta^{\mathrm{o}}\right)}{a^2}w_0^{\mathrm{n}} \qquad (57)$$

$$\varepsilon_2(x = 0, \ y = b) = -\frac{8z\left(1 + \gamma^{\mathrm{o}}\right)}{b^2}w_0^{\mathrm{n}} \qquad (58)$$

and at these positions $\varepsilon_6 = 0$. The corresponding stresses can be calculated using (17).

7.4. Strain energy and resonance frequency

The strain energy of a rectangular plate ($c = b/a$), W, is calculated directly from (28) by evaluating the integrals involved using (17) and (20). The result for a plate of Type V is

$$W = \frac{4096h^3 w_0{}^2}{a^2} \times$$
$$\begin{pmatrix} \frac{c\left(429\beta^2 + 26\beta(\gamma+11) + 7\gamma(3\gamma+26) + 13\left(5\delta^2+77\right)\right)}{4729725} \\ \frac{4\left(9\left(\beta^2+\gamma^2+11\right)+11\delta^2\right)}{3274425c} \\ \frac{4\delta(11\beta+3\gamma-33)}{1091475} \\ \frac{21\beta^2 + 26\beta(\gamma+7) + 13\left(11\gamma(3\gamma+2)+5\delta^2+77\right)}{4729725c^3} \\ \frac{4\delta(3\beta+11(\gamma-3))}{1091475c^2} \\ \frac{8\left(9\left(\beta^2+\gamma^2+11\right)+11\delta^2\right)}{3274425c} \end{pmatrix} \cdot \begin{pmatrix} C_{11}^{\mathrm{eff}} \\ C_{12}^{\mathrm{eff}} \\ C_{13}^{\mathrm{eff}} \\ C_{22}^{\mathrm{eff}} \\ C_{23}^{\mathrm{eff}} \\ C_{33}^{\mathrm{eff}} \end{pmatrix}$$
$$(59)$$

Parameter
$\dfrac{a^4 D_a}{p}\lambda_{00}^{\mathrm{n}} = \dfrac{77\left(5720k_4^2+13c^4\left(13k_2+4c^2\right)\left(7k_2+110c^2\right)+2k_4\left(9477k_2c^2+146072c^4\right)\right)}{128\left(100100k_4^3+259480k_2k_4^2c^2+k_4\left(77363k_2^2+3338540k_4\right)c^4+22k_2\left(169k_2^2+65328k_4\right)c^6+\left(77363k_2^2+3338540k_4\right)c^8+259480k_2c^{10}+100100c^{12}\right)}$
$\dfrac{a^6 D_a}{p}\lambda_{20}^{\mathrm{n}} = \dfrac{1001\left(2860k_4^2+2470k_2k_4c^2+\left(143k_2^2+108k_4\right)c^4+44k_2c^6\right)}{128\left(100100k_4^3+259480k_2k_4^2c^2+k_4\left(77363k_2^2+3338540k_4\right)c^4+22k_2\left(169k_2^2+65328k_4\right)c^6+\left(77363k_2^2+3338540k_4\right)c^8+259480k_2c^{10}+100100c^{12}\right)}$
$\dfrac{a^6 D_a}{p}\lambda_{02}^{\mathrm{n}} = \dfrac{1001\left(44k_2k_4+\left(143k_2^2+108k_4\right)c^2+2470k_2c^4+2860c^6\right)}{128\left(100100k_4^3+259480k_2k_4^2c^2+k_4\left(77363k_2^2+3338540k_4\right)c^4+22k_2\left(169k_2^2+65328k_4\right)c^6+\left(77363k_2^2+3338540k_4\right)c^8+259480k_2c^{10}+100100c^{12}\right)}$
$\beta^{\mathrm{n}} = \dfrac{\lambda_{20}^{\mathrm{n}}}{\lambda_{00}^{\mathrm{n}}}a^2 = \dfrac{13\left(2860k_4^2+2470k_2k_4c^2+143k_2^2c^4+108k_4c^4+44k_2c^6\right)}{5720k_4^2+18954k_2k_4c^2+1183k_2^2c^4+292144k_4c^4+18954k_2c^6+5720c^8}$
$\gamma^{\mathrm{n}} = \dfrac{\lambda_{02}^{\mathrm{n}}}{\lambda_{00}^{\mathrm{n}}}b^2 = \dfrac{13c^2\left(44k_2k_4+\left(143k_2^2+108k_4\right)c^2+2470k_2c^4+2860c^6\right)}{5720k_4^2+13c^4\left(13k_2+4c^2\right)\left(7k_2+110c^2\right)+2k_4\left(9477k_2c^2+146072c^4\right)}$

Table 4: Parameters for the three term Galerkin expression, (52), for the deflection. These expressions are valid for the plate types I, II and III. The aspect ratio of the plate is $c = b/a$.

Type	w_0^{n}
III	$\dfrac{77a^4c^4\left(5720c^8+18954c^6k_2+18954c^2k_2k_4+5720k_4^2+c^4\left(1183k_2^2+292144k_4\right)\right)p}{128D_a\left(100100c^{12}+259480c^{10}k_2+259480c^2k_2k_4^2+100100k_4^3+c^8\left(77363k_2^2+3338540k_4\right)+c^4k_4\left(77363k_2^2+3338540k_4\right)+22c^6\left(169k_2^3+65328k_2k_4\right)\right)}$
II	$\dfrac{77a^4c^4\left(8\left(715+36518c^4+715c^8\right)+18954c^2\left(1+c^4\right)k_2+1183c^4k_2^2\right)p}{128D_a\left(20(1+c^4)(5005+161922c^4+5005c^8)+8c^2(32435+179652c^4+32435c^8)k_2+77363c^4(1+c^4)k_2^2+3718c^6k_2^3\right)}$
I	$\dfrac{77a^4c^4\left(1430+9477c^2+74219c^4+9477c^6+1430c^8\right)p}{128D_a\left(25025+129740c^2+911998c^4+726044c^6+911998c^8+129740c^{10}+25025c^{12}\right)}$

Table 5: Center deflections, (51), calculated using the three term trial function w_n as expressed by (46). The plate types are the same as in Tab. 1. The aspect ratio of the plate is $c = b/a$.

and for brevity the equation is expressed as a dot-product. The resonance frequency of the anisotropic plate is calculated using (29) as

$$\omega^2 = \frac{11h^2}{24a^4c^4\rho[33\beta^2+26\beta(\gamma+11)+11\gamma(3\gamma+26)+13(\delta^2+121)]} \times$$

$$\begin{pmatrix} 9c^4\begin{bmatrix} 429\beta^2+26\beta(\gamma+11) \\ +7\gamma(3\gamma+26)+13\left(5\delta^2+77\right) \end{bmatrix} \\ 52c^2\left(9\left(\beta^2+\gamma^2+11\right)+11\delta^2\right) \\ 3\left(52c^3\delta(11\beta+3\gamma-33)\right) \\ 3\begin{bmatrix} 21\beta^2+26\beta(\gamma+7) \\ +13\left(11\gamma(3\gamma+2)+5\delta^2+77\right) \end{bmatrix} \\ 52c\delta(3\beta+11(\gamma-3)) \\ 104c^2\left(9\left(\beta^2+\gamma^2+11\right)+11\delta^2\right) \end{pmatrix} \cdot \begin{pmatrix} C_{11}^{\mathrm{eff}} \\ C_{12}^{\mathrm{eff}} \\ C_{13}^{\mathrm{eff}} \\ C_{22}^{\mathrm{eff}} \\ C_{23}^{\mathrm{eff}} \\ C_{33}^{\mathrm{eff}} \end{pmatrix}.$$
(60)

The strength of the Rayleigh-Ritz method is, that even with an approximate mode shape an accurate result is obtained. As the overall deflection surface is described by $\left(x^2-a^2\right)^2\left(y^2-b^2\right)^2$ it can be expected that a simple, but accurate, expression for the resonance frequency can be obtained by setting $\beta = \gamma = \delta = 0$. This leads to

$$\omega^2 = \left(7c^4C_{11}^{\mathrm{eff}}+4c^2C_{12}^{\mathrm{eff}}++7C_{22}^{\mathrm{eff}}+8c^2C_{33}^{\mathrm{eff}}\right)\frac{3h^2}{8a^4c^4\rho}.$$
(61)

As will be seen in Sec. 11 this is an excellent approximation.

7.5. Isotropic plates

For the isotropic (i.e. $k_1 = k_3 = 0$, $k_2 = 2$, $k_4 = 1$) square plate, $a = b = L$, we find

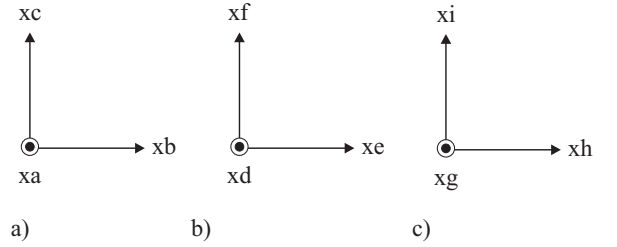$$\beta^{\mathrm{n}} = \gamma^{\mathrm{n}} = 78/269$$
(62)

Figure 4: a) Coordinate system used for (001) silicon substrates. b) Coordinate system used for (011) silicon substrates. c) Coordinate system used for (111) silicon substrates.

and the center deflection (51) becomes

$$w_0^{\mathrm{n}} = \frac{20713}{1025280}\frac{L^4p}{D_i}.$$
(63)

The difference between this result and (5) is only 0.2% which is a sufficient accuracy for most practical applications. The center deflection, (50), calculated from the one term solution, on the other hand, differs by 5%.

8. Silicon substrates

We now consider the mechanical properties of silicon (001), (011) and (111) substrates. For these substrates, the coordinate systems used are shown in Fig. 4.

8.1. Stiffness and compliance for Si

For silicon, having cubic symmetry in the crystallographic coordinate system, the effective compliance matrix

10

Coef.	Resistivity/Doping level	
	150 Ω-cm $\sim 2.8 \times 10^{13}$ cm^{-3}	3.26 mΩ-cm $\sim 2.1 \times 10^{19}$ cm^{-3}
c_{11}^{c}	165.64 GPa	163.94 GPa
c_{12}^{c}	63.94 GPa	64.77 GPa
c_{44}^{c}	79.51 GPa	79.19 GPa
s_{11}^{c}	7.691×10^{-12} Pa^{-1}	7.858×10^{-12} Pa^{-1}
s_{12}^{c}	-2.1420×10^{-12} Pa^{-1}	-2.2254×10^{-12} Pa^{-1}
s_{44}^{c}	12.577×10^{-12} Pa^{-1}	12.628×10^{-12} Pa^{-1}

Table 6: The room temperature stiffness coefficients for n-type crystalline silicon were measured by [35] at two different resistivities. The experimental relative uncertainty is ±0.02%. The corresponding compliance values were calculated using (8). The conversion from resistivity to doping level was performed using ASTM F723 [36].

Substrate	Rotation matrix $\boldsymbol{a}=\boldsymbol{a}(\psi)$
Si(001) $\phi=0$ $\theta=0$	$\begin{pmatrix} \cos\psi & \sin\psi & 0 \\ -\sin\psi & \cos\psi & 0 \\ 0 & 0 & 1 \end{pmatrix}$
Si(011) $\phi=\pi$ $\theta=\pi/4$	$\begin{pmatrix} -\cos\psi & -\frac{\sin\psi}{\sqrt{2}} & \frac{\sin\psi}{\sqrt{2}} \\ \sin\psi & -\frac{\cos\psi}{\sqrt{2}} & \frac{\cos\psi}{\sqrt{2}} \\ 0 & \frac{1}{\sqrt{2}} & \frac{1}{\sqrt{2}} \end{pmatrix}$
Si(111) $\phi=\frac{3}{4}\pi$ $\theta=$ $\cos^{-1}\frac{1}{\sqrt{3}}$	$\begin{pmatrix} -\frac{\cos\psi}{\sqrt{2}}-\frac{\sin\psi}{\sqrt{6}} & \frac{\cos\psi}{\sqrt{2}}-\frac{\sin\psi}{\sqrt{6}} & \sqrt{\frac{2}{3}}\sin\psi \\ -\frac{\cos\psi}{\sqrt{6}}+\frac{\sin\psi}{\sqrt{2}} & -\frac{\sin\psi}{\sqrt{2}}-\frac{\cos\psi}{\sqrt{6}} & \sqrt{\frac{2}{3}}\cos\psi \\ \frac{1}{\sqrt{3}} & \frac{1}{\sqrt{3}} & \frac{1}{\sqrt{3}} \end{pmatrix}$

Table 7: Rotation matrices for (001), (011) and (111) silicon substrates, respectively.

is given by

$$\boldsymbol{S}_{\text{eff}}^{c} = \begin{pmatrix} s_{11}^{c} & s_{12}^{c} & 0 \\ s_{12}^{c} & s_{11}^{c} & 0 \\ 0 & 0 & s_{44}^{c} \end{pmatrix}. \tag{64}$$

The numerical values of the compliance and stiffness elements (both having a relative uncertainty of ±0.02%), as measured by [35], for silicon are listed in Tab. 6. These values depend on the resistivity and for highly doped silicon the stiffness elements are around 1% lower than for low doped silicon.

In order to calculate the effective compliance matrix in the rotated plate coordinate system the elements of the rotation matrices, (9), needs to be found. These are shown in Tab. 7 for plates on (001), (011) and (111) silicon substrates. By performing the transformation in (13) it is found that the effective compliance matrix in the plate coordinate system can be written as

$$\boldsymbol{S}_{\text{eff}} = \boldsymbol{S}_{\text{eff}}^{c} + \left(s_{11}^{c} - s_{12}^{c} - \frac{1}{2}s_{44}^{c} \right) \boldsymbol{\Delta} \tag{65}$$

The matrix $\boldsymbol{\Delta}$ contains all the information about the rotation. The matrix $\boldsymbol{\Delta}$ is listed in Tab. 8 for (001), (011) and (111) silicon substrates, respectively.

Inspection of the matrix $\boldsymbol{\Delta}$ clearly reveals the anisotropy of the silicon crystal:

1. The silicon (001) substrate belongs to the tetragonal crystal family. The crystal class is tetragonal-dipyramidal and the crystal class expressed in Hermann–Mauguin notation (also known as the international notation) is $4/m$. When a plate on the (001) silicon substrate is aligned to the <100> directions, $\psi = 0$ or $\psi = \pi/2$, the compliance matrix has cubic symmetry whereas an orthotropic symmetry is obtained when the plate is aligned to <110> directions, i.e. $\psi = \pi/4$.

2. The structure of the compliance matrix is more complicated for the (011) silicon substrate which belongs to the monoclinic crystal system having the crystal class $2/m$ known as monoclinic-prismatic. When a plate is aligned to the substrate axis, $\psi = 0$, the compliance matrix has orthotropic symmetry.

3. The silicon (111) substrate belongs to the hexagonal crystal family. The crystal system is trigonal and the crystal class is $\bar{3}$ also known as rhombohedral. Thin plates made on the silicon (111) substrate will behave as isotropic plates since trigonal and isotropic materials have the same structure of the compliance matrix when the condition of plane stress is fulfilled.

In conclusion, thin plates on the (001), (011) and (111) silicon substrates are of plate Type IV, V and I, respectively.

8.2. Plate equation coefficients for Si

Fig. 5 shows values of the plate equation coefficients k_1 to k_4 calculated using the expressions in Tab. 3 combined with the expressions for the effective compliance, given in (65) and Tab. 8, and selected values of the plate equation coefficients are summarized in Tab. 9. The relative errors due to the uncertainty in the compliance values are in the range of 0.01%–0.07%.

On the (001) silicon substrate the coordinate system, shown in Fig. 4a, is aligned such that the x–, y- and z-axis are oriented along the [100], [010] and [001] directions respectively. The coefficient k_4 is constant and equal to one whereas k_2 varies from 2.81 along the <001> directions to a minimum of 1.32 along the <011> directions. The coefficients k_1 and k_3 have extrema for $\psi = n\pi/8$ where n is an uneven integer and they have a value of zero along the <001> and <011> directions. On the (001) silicon substrate $k_1 = -k_3$.

On the (011) silicon substrate the coordinate system is aligned such that the x–, y- and z-axis are oriented along the [$\bar{1}$00], [0$\bar{1}$1] and [011] directions respectively. The coefficient k_4 varies from 1.30 along the <001> directions to 0.77 along the <011> directions with a value of one at $\psi = \pi/4$. The coefficient k_2 varies from 2.92 along the <001> directions to 2.25 along the <011> directions with a minimum of 1.51. On the (011) substrate the coefficients k_1 and k_3 have a value of zero at $\psi = 0$ and $\psi = \pi/2$.

11

Substrate	Δ
(001)	$\begin{pmatrix} \frac{1}{4}(-1+\cos(4\psi)) & \frac{1}{4}(1-\cos(4\psi)) & -\frac{1}{2}\sin(4\psi) \\ \frac{1}{4}(1-\cos(4\psi)) & \frac{1}{4}(-1+\cos(4\psi)) & \frac{1}{2}\sin(4\psi) \\ -\frac{1}{2}\sin(4\psi) & \frac{1}{2}\sin(4\psi) & 1-\cos(4\psi) \end{pmatrix}$
(011)	$\begin{pmatrix} \frac{1}{16}(-7+4\cos(2\psi)+3\cos(4\psi)) & -\frac{3}{16}(-1+\cos(4\psi)) & \frac{1}{8}(-2\sin(2\psi)-3\sin(4\psi)) \\ -\frac{3}{16}(-1+\cos(4\psi)) & \frac{1}{16}(-7-4\cos(2\psi)+3\cos(4\psi)) & \frac{1}{8}(-2\sin(2\psi)+3\sin(4\psi)) \\ \frac{1}{8}(-2\sin(2\psi)-3\sin(4\psi)) & \frac{1}{8}(-2\sin(2\psi)+3\sin(4\psi)) & -\frac{3}{4}(-1+\cos(4\psi)) \end{pmatrix}$
(111)	$\begin{pmatrix} -\frac{1}{2} & \frac{1}{6} & 0 \\ \frac{1}{6} & -\frac{1}{2} & 0 \\ 0 & 0 & \frac{4}{3} \end{pmatrix}$

Table 8: Δ matrices for (001), (011) and (111) silicon substrates, respectively.

Sub.	ψ	k_1	k_2	k_3	k_4	$12D_\mathrm{a}/h^3$ [GPa]
Si(001)	0	0	$\begin{cases} 2.8133 \pm 0.0006 \\ 2.8559 \pm 0.0006 \end{cases}$	0	1	$\begin{cases} 140.96 \pm 0.03 \\ 138.35 \pm 0.03 \end{cases}$
	$\pi/4$	0	$\begin{cases} 1.3241 \pm 0.0004 \\ 1.2949 \pm 0.0004 \end{cases}$	0	1	$\begin{cases} 169.62 \pm 0.03 \\ 167.96 \pm 0.03 \end{cases}$
Si(011)	0	0	$\begin{cases} 2.9233 \pm 0.0006 \\ 2.9718 \pm 0.0006 \end{cases}$	0	$\begin{cases} 1.2994 \pm 0.0002 \\ 1.3156 \pm 0.0002 \end{cases}$	$\begin{cases} 144.60 \pm 0.03 \\ 142.27 \pm 0.03 \end{cases}$
	$\pi/4$	$\begin{cases} 0.2293 \pm 0.0001 \\ 0.2387 \pm 0.0001 \end{cases}$	$\begin{cases} 1.5222 \pm 0.0003 \\ 1.5036 \pm 0.0003 \end{cases}$	$\begin{cases} 0.2293 \pm 0.0001 \\ 0.2387 \pm 0.0001 \end{cases}$	1	$\begin{cases} 188.80 \pm 0.04 \\ 188.05 \pm 0.04 \end{cases}$
	$\pi/2$	0	$\begin{cases} 2.2497 \pm 0.0002 \\ 2.2589 \pm 0.0002 \end{cases}$	0	$\begin{cases} 0.7695 \pm 0.0001 \\ 0.7601 \pm 0.0001 \end{cases}$	$\begin{cases} 187.89 \pm 0.04 \\ 187.16 \pm 0.04 \end{cases}$
Si(111)	All	0	2	0	1	$\begin{cases} 181.42 \pm 0.04 \\ 180.30 \pm 0.04 \end{cases}$

Table 9: Selected values of the plate coefficients k_1, k_2, k_3, k_4, and the flexural rigidity, $12D_a/h^3$ for silicon (001), (011) and (111) substrates, respectively. The curly braces are used to group calculated values for the two different resistivities shown in Tab. 6. The topmost value is for the highest of the two resistivities.
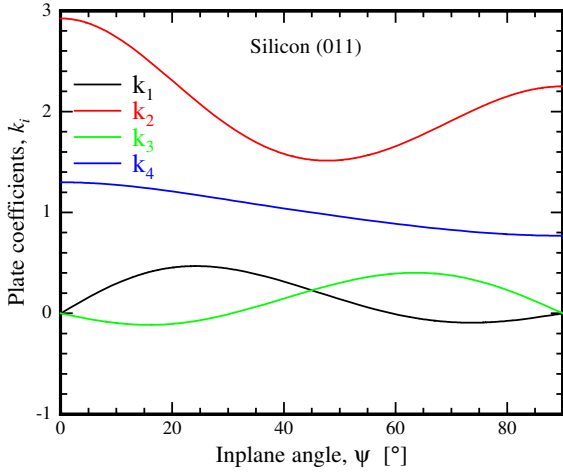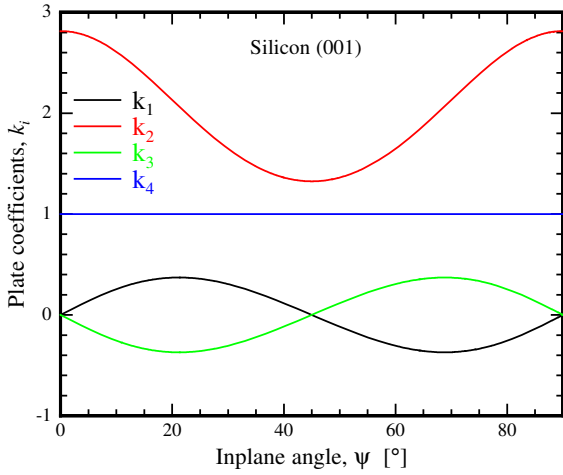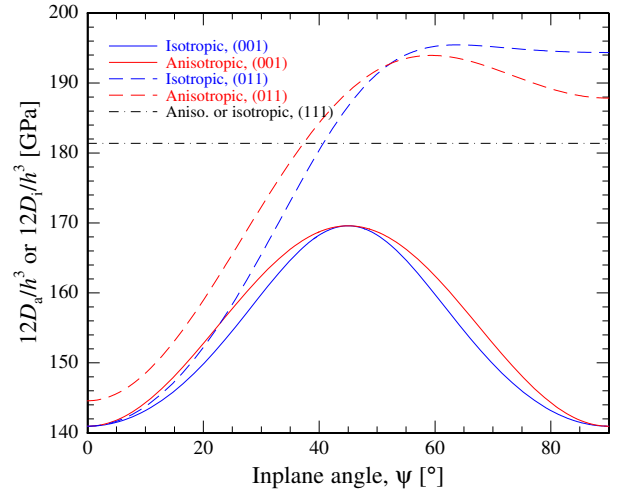
Figure 6: Plot of the isotropic, $12D_{\mathrm{i}}/h^3$, and anisotropic flexural rigidities, $12D_{\mathrm{a}}/h^3$, for (001), (011) and (111) silicon substrates respectively. The values of $12D_{\mathrm{i}}/h^3$ were calculated by evaluating the Young's modulus, (D.1), and the Poisson's ratio, (D.2), corresponding to uniaxial stress in the orientational direction. On the (111) silicon substrate the flexural rigidity is constant.

Figure 5: Plot of the plate equation coefficients k_1–k_4 for (001) and (011) silicon substrates. For silicon (111) all values are constant and $k_1 = k_3 = 0$ whereas $k_2 = 2$ and $k_4 = 1$.

On the (111) silicon substrate the plate equation coefficients are constant with $k_1 = k_3 = 0$, $k_2 = 2$ and $k_4 = 1$, i.e. identical to those for an isotropic plate.

Considering (2) it is seen that $12D_{\mathrm{i}}/h^3$ has a value on the order of the Young's modulus. Therefore, the results for the flexural rigidities are plotted as $12D_{\mathrm{i}}/h^3$ or $12D_{\mathrm{a}}/h^3$ and selected values are given in Tab. 9. The values of the anisotropic flexural rigidity, expressed as $12D_{\mathrm{a}}/h^3$, are shown in Fig. 6 together with the isotropic flexural rigidity, $12D_{\mathrm{i}}/h^3$. The values of $12D_{\mathrm{a}}/h^3$ were calculated using the expressions in Tab. 2, and the values of $12D_{\mathrm{i}}/h^3$ were calculated from the expressions in appendix Appendix D by evaluating the Young's modulus, (D.1), and the Poisson's ratio, (D.2), corresponding to uniaxial stress in the orientational direction. It is noticed, that the two flexural rigidities, D_{i} and D_{a}, are quite similar and the maximum

difference between them is less than 2% on the (001) and less than 4.5% on the (011) silicon substrate. On the (111) silicon substrate $D_{\mathrm{a}} = D_{\mathrm{i}}$.

9. Circular silicon plates

We now consider circular plates made on different silicon substrates. Analytical and FEM calculations were performed for thin clamped circular and elliptic plates made on (001), (011) and (111) silicon substrates. In the FEM calculations, the anisotropy was taken into account by using the appropriate 6×6 stiffness matrix calculated directly from (12) using the stiffness values given in Tab. 6.

9.1. Center deflection

Fig. 7 shows the normalized center deflection for a circular plate on the (001), (011) and (111) silicon substrates. The deflection is normalized to the value of the FEM center deflection for a plate on the (111) silicon substrate. As expected from symmetry, the exact solution, (31), yields a constant deflection, regardless of the orientation, ψ, on all substrates. Therefore, any single set of values from Tab 9 for k_2, k_4 and D_{a} can be used.

Using directional values for the Young's modulus and Poisson's ratio, (D.1) and (D.2), to calculate the center deflection using the isotropic expression (4) leads to maximum errors of 10% and 26% in the center deflection for plates on (001) and (011) silicon substrates, respectively. Clearly, it is an advantage to use the anisotropic approach. Finally, it is noted, that circular plates on (001) silicon substrates have a 17% larger deflection than plates with the same geometry but made on (111) silicon substrates.
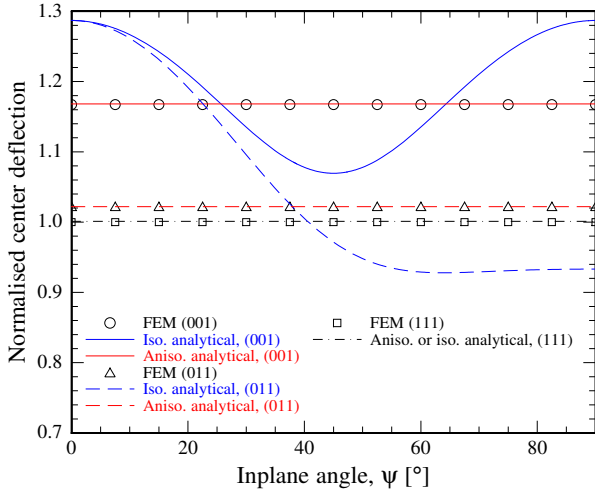
13

Figure 7: Normalized center deflections for a thin clamped circular plate as function of inplane rotation angle on (001), (011) and (111) silicon substrates, respectively. The center deflections are normalized to the center deflection on (111) silicon as calculated by FEM. The curves for the isotropic analytical center deflections were calculated using (2), (4), (D.1) and (D.2). There is an excellent agreement between the center deflections calculated using the analytical anisotropic equation, (31), and the FEM results. The maximum relative difference between the two results is less than 0.1%.

For plates on (011) silicon substrates, the corresponding number is 2%.

Fig. 7 also shows the result of a finite element simulation taking the anisotropic nature of silicon into account. As expected, there is an excellent agreement between the finite element calculation and the exact anisotropic polynomial solution and the maximum relative difference between the two results is less than 0.1%. For plates on (111) silicon substrates, the anisotropic approach yields, as expected, the same result as obtained from the isotropic plate equation.

9.2. Deflection

Fig. 1 shows a cross section ($y = 0$) of the calculated and simulated deflection surfaces for a circular plate on a silicon (001) substrate normalized to the center deflection of the anisotropic deflection surface. The datapoints represent the results from the finite element calculation which is in excellent agreement, difference in center deflection of less than 0.1%, with the deflection calculated from (3) and (31). Fig. 1 also shows two cross sections ($y = 0$) of the deflection surface, calculated using the isotropic expression (4) together with (3), where the Young's modulus, (D.1), and Poisson's ratio, (D.2), were chosen corresponding to the [100] ($E = 130.0$ GPa, $\nu = 0.279$) or [110] directions ($E = 169.0$ GPa, $\nu = 0.062$) on the (001) silicon substrate. Using the isotropic parameters yields an error of around 10%. Clearly, it is an advantage to use the anisotropic approach as presented in this article.
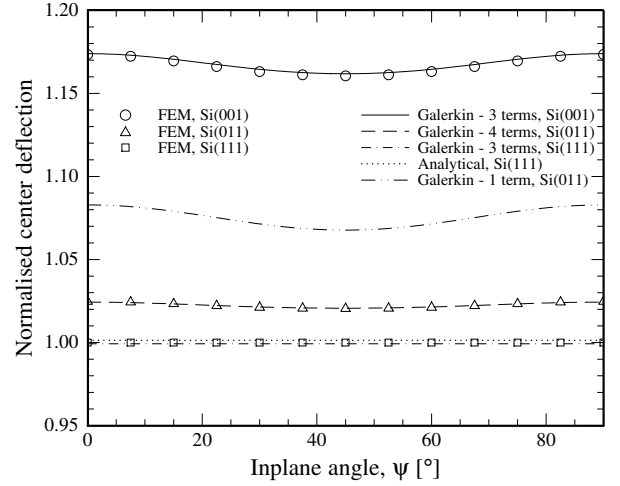

Figure 8: Normalized center deflections for a square plate as function of inplane rotation angle, ψ, on silicon (001), (011) and (111) substrates, respectively. The center deflections are normalized to the center deflection on the (111) silicon substrate as calculated by FEM. The different solid and dashed lines show results from a Galerkin calculation. Using only one term in a series expansion of the deflection, (45), leads to an error in the center deflections of around 5% compared to the FEM results. This is illustrated by the center deflection for a square plate on a silicon (011) substrate. However, using three, (46), or four, (47), terms in the expansion leads to an excellent match between the analytical center deflections, (51) and (54), and the FEM results. For the (111) silicon plate, the isotropic expression, (5), shown as the dotted line is in perfect agreement with the FEM results. The maximum difference between the analytical and FEM result for the center deflection is less than 0.1% on all substrates investigated.
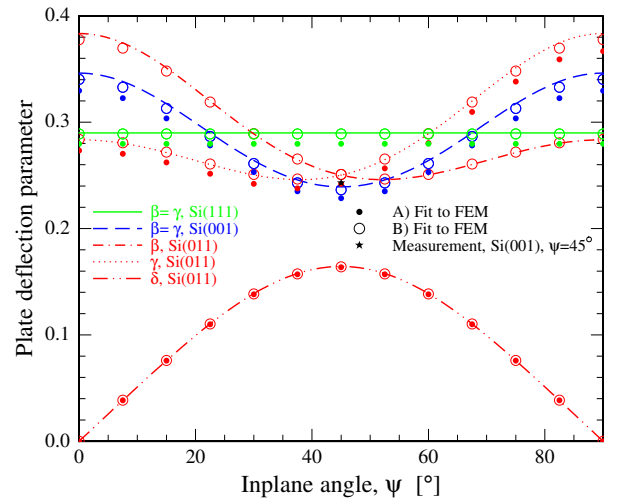

Figure 9: Plate deflection parameters (β, γ and δ) for square plates on silicon (001), (011) and (111) substrates, respectively. The curves represents the analytical results and the symbols corresponds to the corresponding values as extracted by non linear least squares fitting of (55) to the deflection surfaces calculated by FEM. The solid star represents the value found in [37] for a square plate on a Si(001) substrate aligned to the [110] direction. A) and B) indicate the type of fit used.

14

Substrate:	Si (001)		Si (011)			Si (111)
ψ	0	$\pi/4$	0	$\pi/4$	$\pi/2$	All
Resistivity, 150 Ω-cm						
$w_0 D_\mathrm{a}/(L^4 p)$	0.018441	0.021961	0.016508	0.021475	0.021448	0.020202
β	0.34615	0.23920	0.38334	0.25022	0.28343	0.28996
γ	0.34615	0.23920	0.28343	0.25022	0.38334	0.28996
δ	0	0	0	0.16329	0	0
Resistivity, 3.26 mΩ-cm						
$w_0 D_\mathrm{a}/(L^4 p)$	0.018357	0.022045	0.016347	0.021531	0.021506	0.020202
β	0.3490	0.2369	0.38800	0.24842	0.28309	0.28996
γ	0.3490	0.2369	0.28308	0.24842	0.38800	0.28996
δ	0	0	0	0.17178	0	0

Table 10: Values of the plate deflection parameters (α, β and δ) and expressions for the center deflections for square plates on silicon (001), (011) and (111) substrates, respectively, aligned to different directions. The relative uncertainty in the calculated parameters are below $\pm 0.02\%$.

10. Square silicon plates

We now consider square plates ($c = 1$, $a = b = L$) made on silicon (001), (011) and (111) substrates, respectively. To investigate the deflection behavior of such plates the Galerkin expressions derived in section 7 were compared to FEM simulations. Calculated values of the center deflection and plate deflection parameters (β, γ and δ) for selected orientations of a square silicon plate are listed in Tab. 10 and the variation of these parameters with inplane rotation angle of the plate are shown in figures 8 and 9.

10.1. Center deflection

Center deflections for selected directions on (001), (011) and (111) silicon substrates, respectively, are given in Tab. 10. Fig. 8 shows the center deflection of square plates on (001), (011) and (111) silicon substrates as a function of the in plane rotation angle ψ of the square. There is a very good agreement between the FEM results and the analytically calculated center deflections where the three term expression (51) was used for plates on the (001) and (111) substrate and the four term expression (54) for plates on the (011) substrate. The maximum difference between the analytical and FEM result for the center deflection is less than 0.1% on all substrates investigated. Using only one term, however, in the expansion for the center deflection, (45), leads to a difference of around 5%.

10.1.1. Silicon (001)

Plates on silicon (001) substrates are generally of Type IV, and the plate equation coefficients have the special property that $k_1 = -k_3$ and $k_4 = 1$. However, when plates on this substrate are aligned to <100> or <110> directions the plate type is II (cubic) and III (orthotropic), respectively. For a *square* plate on a silicon (001) substrate these special properties leads to the simple result that the plate deflection parameters are identical to those of a square cubic plate. Therefore, the results of section

(7.2.2) can be applied and the center deflection, (51), is simply given by

$$w_0 = \frac{77\,(1432 + 91k_2)}{256\,(16220 + 11k_2\,(329 + 13k_2))}\,\frac{L^4 p}{D_\mathrm{a}}. \qquad (66)$$

It is noticed, that for square plates on silicon (001) substrates only the plate coefficient k_2 needs to be calculated. Fig. 8 shows how the center deflection depends on the inplane rotation of the plate. The center deflection is almost constant and varies with only 1% having maximum when the plate is aligned to the [100] direction and minimum when the plate is aligned to the [110] direction. The center deflection is normalized to the center deflection of a square plate on a silicon (111) substrate as calculated by FEM and the figure demonstrates the excellent agreement, difference less than 0.04%, between the analytical expression for the center deflection, (66), and the FEM calculation.

10.1.2. Silicon (011)

Plates on silicon (011) substrates are of Type IV and thus highly anisotropic. The deflection of such plates can be calculated based on the results of section (7.2.3). The center deflection is given by (54) and in general involves all four plate equation coefficients, k_1–k_4. As seen in Fig. 8 the center deflection is almost constant and varies only 0.4% with the inplane rotation angle.

10.1.3. Silicon (111)

Plates fabricated on silicon (111) substrates behave as isotropic plates, Type I. The center deflection can be calculated from (63) or (2) using values of the Young's modulus, (D.5), and Poisson's ratio, (D.9), from Appendix Appendix D. The center deflection is constant with inplane rotation angle as shown in Fig. 8.

10.2. Deflection

The deflection surface of square plates can be easily calculated using the results of section 7.2.2 and 7.2.3. The

deflection depends on the values of the plate deflection parameters (β, γ and δ) and the values of these are shown in Fig. 9 and selected values are given in Tab. 10.

10.2.1. Silicon (001)

The deflection of plates on the silicon (001) substrate is described by (52) and depends only on β^{n} and γ^{n}. From Tab. (4) and (53) we obtain

$$\beta^{\mathrm{n}} = \gamma^{\mathrm{n}} = \frac{182 + 143k_2}{1432 + 91k_2}. \tag{67}$$

The variation of these parameters with inplane rotation angle is shown in Fig. 9. The highest values ($\beta^{\mathrm{n}} = \gamma^{\mathrm{n}} = 0.34615$) are obtained when the plate is aligned to the $<100>$ directions, $\psi = 0$, whereas the minimum value ($\beta^{\mathrm{n}} = \gamma^{\mathrm{n}} = 0.23920$) is found when the plate is aligned to $<110>$ direction, $\psi = \pi/4$.

Fig. 10 compares a cross section, $y = 0$, obtained from (52) with a FEM calculation of the deflection of a square (001) silicon plate where the edges of the plate are aligned to the $<110>$ directions, i.e. for $\psi = \pi/4$. There is an excellent agreement between the analytical result, shown as the full line, and the FEM result as show by the open circles. The difference in the calculated center deflections are only 0.1%. The figure also shows two cross sections ($y = 0$) of the deflection surfaces, calculated using the isotropic expressions (62) and (63) together with (52), where the Young's modulus, (D.1), and Poisson's ratio, (D.2), were chosen corresponding to the [100] ($E = 130.0$ GPa, $\nu = 0.2785$) or [110] directions ($E = 169.0$ GPa, $\nu = 0.0625$) on the (001) silicon substrate. Using the isotropic expressions yields, as for the circular plate, an error of around 10%.

10.2.2. Silicon (011)

For plates on the silicon (011) substrate the deflection is given by (55) and depends on the plate deflection parameters β^{o}, γ^{o} and δ^{o} as given by (56). On this substrate β^{o} is in general different from γ^{o} and the value of δ^{o} is non-zero except for $\psi = 0$ and $\psi = \pi/2$ where the plates have an orthotropic symmetry.

10.2.3. Silicon (111)

On the silicon (111) substrate, the deflection is given by (52) and the plate deflection parameters are identical to those for an isotropic plate as given by (62).

10.2.4. Comparison to FEM deflection and measurements

Fig. 9 also compares the calculated plate deflection parameters with corresponding parameters obtained by non-linear least squares fitting of expressions (52), for plates on (001) and (111) silicon substrates, and (55), for plates on the (011) silicon substrate, to 3D deflection surfaces calculated by FEM. The solid star represents the value found by measuring the deflection of a square plate on a Si(001) substrate aligned to the [110] direction where it was found that
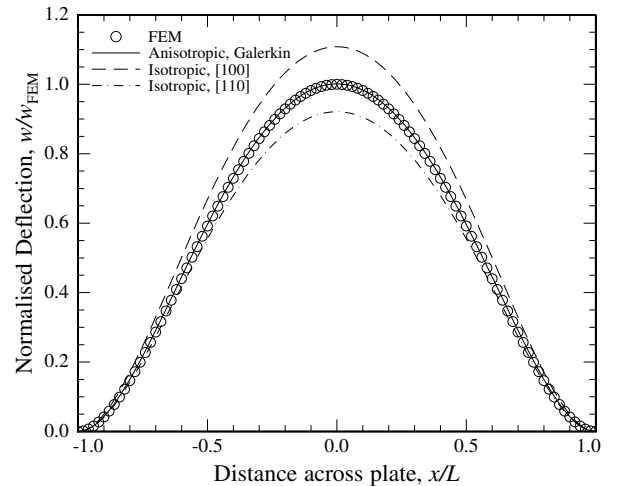

Figure 10: The figure compares (46) with a FEM calculation of the deflection of a square (001) silicon plate where the edges of the plate are aligned to the $<100>$ directions. The deflection is normalized to the FEM center deflection and the figure shows the excellent agreement between the analytical anisotropic expression and the FEM calculation. The dashed and dot-dashed curves, corresponds to the isotropic result, (63) using values of the Poisson's ratio and Young's modulus corresponding to the [100] and [110] directions on the (001) silicon substrate, respectively. Using the isotropic plate equation leads to deviations of the center deflection of around 10% whereas the analytical anisotropic result is in excellent agreement with the FEM calculation.

$\beta^{\mathrm{n}} = 0.243$ [37] in very good agreement with the Galerkin result of $\beta^{\mathrm{n}} = 0.23920$. The open circles represents the obtained results when both the center deflection and the plate deflection parameters were varied during fitting (case A), whereas the solid circles represents the case where only the plate deflection parameters were varied (case B). As the correlation between the center deflection and β and γ is large (~ 0.6) the calculated parameters are closer to the Galerkin results (shown by the different lines) when also the center deflection is varied. For the plate deflection parameter δ^{o} the correlation with the center deflection is small (~ 0.02) and the two fitting procedures yield essentially the same results (difference less than 0.3%) in close agreement (difference less than 0.5%) with the Galerkin expression (56) for δ^{o}.

To investigate how small changes in the plate deflection parameters influences the deflection surface we consider a square plate aligned to $<110>$ directions on a silicon (001) substrate. The results from the two fits, A and B, are shown in Tab. 11. The difference in β^{n} found using procedure A and B is 3% and the difference between the results obtained from the fit and the Galerkin expression (67) is 1% and 4% for case A and B respectively. The difference between the Galerkin value and the measurement is 1.6%.

These differences have, however, little effect on the shape of the deflection surface. The full width half maximum of the surface differs by less than 0.1% whereas the

16

Parameter	Case A	Case B	Galerkin (67)	Exp. [37]
β^{n}	0.23640	0.22850	0.23920	0.243

Table 11: The plate deflection parameter β^{n} was determined by fitting (52) to the 3D deflection surface calculated by FEM for a square plated aligned to the [110] direction on a silicon (001) surface. In Case A both β^{n} and w_0 was varied whereas only β^{n} was varied in Case B.

volume of the deflection surfaces differs by less than 0.2%. If the plate was used as an electrode in a capacitive device having a square plate with $L/h = 100$ and a gap of $3h/5$ the difference in the calculated values of β^{n} will only lead to a difference in capacitance of 0.03% when the center deflection is $1/3$ of the gap. Likewise, the change in resonance frequency as calculated by (60) for a device having $L/h = 100$ is only 0.06%. Therefore, the analytical results from the Galerkin calculation can be safely used to predict the deflection surface of the plate.

11. Examples

We now consider circular and square plates fabricated on a silicon (001) substrate having the plate coordinate system aligned to the [110] direction, i.e. aligned to the primary flat on the wafer such that $\psi = \pi/4$. Expressions for the center deflection, strain energy and resonance frequency will be given expressed in terms of dimensions of the plates and appropriate multiplication factors given in Tab. 12. These factors are calculated by using values from tables, 6, 9, and 10, respectively, together with the density of silicon, $\rho = 2330 \ \mathrm{kg \cdot m^{-3}}$.

11.1. Compliance

In this case the effective compliance matrix is given by (65) which using (64) together with Tab. 8 yields

$$S^{\mathrm{eff}}_{\mathrm{Si(001),<110>}} =$$
$$\begin{pmatrix} \frac{2(s^{\mathrm{c}}_{11}+s^{\mathrm{c}}_{12})+s^{\mathrm{c}}_{44}}{4} & \frac{s^{\mathrm{c}}_{11}+s^{\mathrm{c}}_{12}}{2} - \frac{s^{\mathrm{c}}_{44}}{4} & 0 \\ \frac{s^{\mathrm{c}}_{11}+s^{\mathrm{c}}_{12}}{2} - \frac{s^{\mathrm{c}}_{44}}{4} & \frac{2(s^{\mathrm{c}}_{11}+s^{\mathrm{c}}_{12})+s^{\mathrm{c}}_{44}}{4} & 0 \\ 0 & 0 & 2(s^{\mathrm{c}}_{11} - s^{\mathrm{c}}_{12}) \end{pmatrix} \quad (68)$$

and the plate is of Type III having an orthotropic symmetry. The effective stiffness is

$$C^{\mathrm{eff}}_{\mathrm{Si(001),<110>}} = S^{\mathrm{eff} \, -1}_{\mathrm{Si(001),<110>}} =$$
$$\begin{pmatrix} \frac{1}{s^{\mathrm{c}}_{44}} + \frac{1}{2(s^{\mathrm{c}}_{11}+s^{\mathrm{c}}_{12})} & \frac{1}{2(s^{\mathrm{c}}_{11}+s^{\mathrm{c}}_{12})} - \frac{1}{s^{\mathrm{c}}_{44}} & 0 \\ \frac{1}{2(s^{\mathrm{c}}_{11}+s^{\mathrm{c}}_{12})} - \frac{1}{s^{\mathrm{c}}_{44}} & \frac{1}{s^{\mathrm{c}}_{44}} + \frac{1}{2(s^{\mathrm{c}}_{11}+s^{\mathrm{c}}_{12})} & 0 \\ 0 & 0 & \frac{1}{2s^{\mathrm{c}}_{11}-2s^{\mathrm{c}}_{12}} \end{pmatrix}. \quad (69)$$

Factor	High resistivity	Low Resistivity	Unit
κ_1	1.2074×10^{-12}	1.2242×10^{-12}	Pa^{-1}
κ_2	4.3365×10^{11}	4.2769×10^{11}	$\mathrm{J/m^3}$
κ_3	5.9242×10^{8}	5.8429×10^{8}	$\mathrm{m^2/s}$
κ_4	1.5537×10^{-12}	1.5690×10^{-12}	Pa^{-1}
κ_5	3.9117×10^{11}	3.8564×10^{11}	$\mathrm{J/m^3}$
κ_6	4.6626×10^{8}	4.6003×10^{8}	$\mathrm{m^2/s}$
κ_7	4.5448×10^{8}	4.4844×10^{8}	$\mathrm{m^2/s}$

Table 12: Scaling factors to be used in (70)-(77).

11.2. Circular plates

For circular plates, the center deflection, (31), strain energy, (35) and resonance frequency, (37), becomes

$$w_0|_{\mathrm{Si(001)}} = \kappa_1 \frac{a^4}{h^3} p \quad (70)$$

$$W|_{\mathrm{Si(001)}} = \kappa_2 \frac{h^3 w_0^2}{a^2} = \kappa_2 \kappa_1^2 \frac{a^6}{h^3} p^2 \quad (71)$$

$$\omega^2|_{\mathrm{Si(001)}} = \kappa_3 \frac{h^2}{a^4}. \quad (72)$$

11.3. Square plates

We now consider the case where square plates, $a = b = L$, are aligned to the primary flat on a silicon (001) wafer, i.e. along $<110>$ directions corresponding to $\psi = \pi/4$. This type of plate is particularly important as such plates are easily realized by KOH or TMAH etching of (001) silicon. The value of β (for low doped silicon) for this orientation is $\beta = 0.23920$ as obtained from Tab. 10. The center deflection is given by (Tab. 10)

$$w_0|_{\mathrm{Si(001),<110>}} = 0.021961 \frac{L^4}{D_{\mathrm{a}}} p. \quad (73)$$

Using values from Tab. 9 the center deflection can be written as

$$w_0|_{\mathrm{Si(001),<110>}} = \kappa_4 \frac{L^4}{h^3} p.$$

Compared to FEM of a plate having $L/h = 100$ the deflection calculated using this expression differs only 0.1% from the value found by FEM. The deflection surface, for a low doped plate, is given by (52)

$$\frac{w}{w_0}\bigg|_{\mathrm{Si(001),<110>}} = \left[1 - \left(\frac{x}{L}\right)^2\right]^2 \left[1 - \left(\frac{y}{L}\right)^2\right]^2$$
$$\times \left\{1 + 0.23920\left[\left(\frac{x}{L}\right)^2 + \left(\frac{y}{L}\right)^2\right]\right\}. \quad (74)$$

This simple expression for the deflection can be applied to a range of devices including for example calculation of the device capacitance of CMUTs.

The strain energy stored in this plate can be calculated from (59) using tables 9 and 10

$$W|_{\mathrm{Si(001),<110>}} = \kappa_5 \frac{h^3 w_0^2}{L^2} = \kappa_5 \kappa_4^2 \frac{L^6 p^2}{h^3}. \quad (75)$$

For a plate having $L/h = 100$ this equation yields a result being in excellent agreement with a FEM calculation of the strain energy as the calculated value is only 0.35% smaller than the valued predicted by FEM.

The resonance frequency of the plate is calculated using (60), $\beta = 0.23920$, $\rho = 2330 \, \mathrm{kg/m^3}$ and values from Tab. 6

$$\omega^2\big|_{\mathrm{Si}(001),<110>} = \kappa_6 \frac{h^2}{L^4}. \tag{76}$$

Compared to a FEM calculation, using again $L/h = 100$, this expression yield a resonance frequency only 1.2% larger than the value found by FEM. Using the simplified equation for the resonance frequency, (61), and values from Tab. 6 we obtain

$$\omega^2\big|_{\mathrm{Si}(001),<110>} = \kappa_7 \frac{h^2}{L^4} \tag{77}$$

which is only 0.1% smaller than the value found by FEM. The model presented here is clearly in very good agreement with FEM and efficient to use for design and modeling purposes.

12. Conclusion

The anisotropic plate equation was derived for the case of thin crystalline plates in the small deflection approximation where the effects of stress stiffening can be ignored. Using the plane stress assumption, the number of different plate types for crystalline plates are reduced to five based on their effective compliance matrix and plates having trigonal or hexagonal symmetry behave as isotropic plates. The anisotropic plate equation has five parameters that depends on the elastic constants of the crystal: The four plate equation coefficients, k_1 to k_4 and the generalized flexural rigidity, D_a. Expressions for these parameters were determined for any of the five different plate types. The deflection surface of commonly used plate shapes were calculated for the case where the edges of the plates are clamped, and a framework for taking elastic boundary conditions into consideration was established. For circular and elliptic plates exact solutions to the anisotropic plate equation exists. For rectangular and square plates, the Galerkin method was used to determine approximate, yet very accurate, expressions for the deflection. The calculated expressions for the deflection surface, strain energy and resonance frequency are valid for any of the five different plate types, i.e. for plates of any crystal class.

The anisotropic plate equation is very useful for determining the deflection surface, strain energy and resonance frequency of thin plates made on crystalline silicon substrates. The deflection surface, stain energy and resonance frequency were calculated for clamped circular, elliptic, square and rectangular plates on silicon (001), (011) and (111) substrates. For plates made on the trigonal (111) silicon substrates the isotropic plate equation is valid and the mechanical parameters for the plate are given by

the Young's modulus and the Poisson's ratio. However, for plates made on (001) and (011) silicon substrates the anisotropic plate equation must be used, and the mechanical parameters of the plates are described by the plate equation coefficients k_1 to k_4 together with the anisotropic flexural rigidity, D_a. These parameters depend on the orientation of the plate and expressions for these were calculated for the silicon substrates investigated. For circular and elliptic plates an exact solution to the anisotropic plate equation is available, and calculated results are in excellent agreement with finite element modeling. For the square and rectangular plates the expressions for the plate deflection derived using the Galerkin method are useful as approximations and using three terms in a series expansion the maximum difference in center deflection, strain energy and resonance frequency between the analytical results and the results from FEM was at most 0.1%, 0.35% and 0.1% respectively, for a square plate aligned to the [110] direction on a silicon (001) substrate.

Appendix A. Elastic boundary conditions

We now consider a plate with more realistic boundary conditions, i.e. an elastic boundary. The thin plate is attached to a larger block of material which is fixed far away from the edge of the plate as illustrated in Fig. A.11. The effect of this is to make the plate more soft and it will appear to have a larger radius, a_{eff}. In a heuristic way we might write

$$a_{\mathrm{eff}} = a + ch \tag{A.1}$$

where c is a constant that needs to be found. Finite element modelling shows that the effect of an elastic boundary is to increase the center deflection with 2% compared to a clamped plate when the aspect ratio is $a/h = 100$ and this number increases to 11% for an aspect ratio of $a/h = 20$. For the resonance frequency of the plate the corresponding relative decrease in resonant frequencies are 1% and 6%, respectively.

From Eq. 60 and 4 we see, that the resonance frequency of a clamped plate, ω_{clp}, is proportional to h/a^2 whereas the center deflection, $w_{0,\mathrm{clp}}$, is proportional to a^4. Then, the resonance frequency, ω_{eb}, and center deflection, $w_{0,\mathrm{eb}}$, of a plate with an elastic boundary is

$$\omega_{\mathrm{eb}} \propto \frac{h}{a_{\mathrm{eff}}^2} \qquad w_{0,\mathrm{eb}} \propto a_{\mathrm{eff}}^4 \tag{A.2}$$

Therefore,

$$\sqrt{\frac{\omega_{\mathrm{clp}}}{\omega_{\mathrm{eb}}}} = \frac{a_{\mathrm{eff}}}{a} = \frac{a + ch}{a} = 1 + c\frac{h}{a} \tag{A.3}$$

$$\sqrt[4]{\frac{w_{0,\mathrm{eb}}}{w_{0,\mathrm{clp}}}} = \frac{a + ch}{a} = 1 + c\frac{h}{a} \tag{A.4}$$

Based on this, we see that a plot of $\sqrt{\frac{\omega_{\mathrm{clp}}}{\omega_{\mathrm{eb}}}} - 1$ or $\sqrt[4]{\frac{w_{0,\mathrm{eb}}}{w_{0,\mathrm{clp}}}} - 1$ versus h/a is expected to yield a straight line with slope
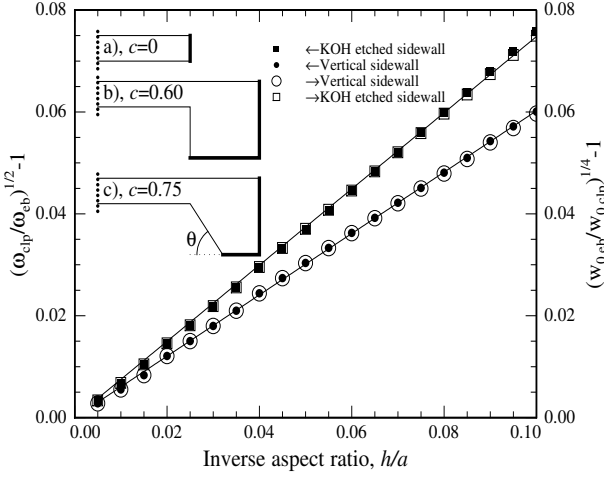
Figure A.11: Based on Eq. A.3 and A.4 a plot of $\sqrt{\frac{\omega_{\mathrm{clp}}}{\omega_{\mathrm{eb}}}} - 1$ (solid symbols) or $\sqrt[4]{\frac{w_{0,\mathrm{eb}}}{w_{0,\mathrm{clp}}}} - 1$ (open symbols) versus h/a is expected to yield a straight line with slope c. The insert shows the three cases considered: a) a clamped plate, b) a plate attached to an elastic support having a vertical sidewall and c) a plate attached to an elastic support having a sidewall with an inclined slope, $\theta = 54.7°$, corresponding to a plate defined by anisotropic etching of silicon using KOH. The thick lines indicate the fixed boundaries and the dotted line shows the axis of the rotational symmetry. In all cases there is an excellent agreement between the model and the data points calculated by FEM. The solid lines are a fit to $c \cdot h/a$.

c. Such plots are shown in Fig. A.11. The resonance frequency and center deflections were calculated by the FEM tool COMSOL for a circular isotropic silicon plate using rotational symmetry and the aspect ratios used in the calculations were in the range $a/h \in [10 \ldots 200]$. Three cases were considered: a) a clamped plate, b) a plate attached to an elastic support having a vertical sidewall and c) a plate attached to an elastic support having a sidewall with an inclined slope, $\theta = 54.7°$, corresponding to a plate defined by anisotropic etching of silicon using KOH. There is a very good agreement with the model and a value of $c = 0.60$ is found for the support with the vertical sidewall and $c = 0.75$ is found for the structure with the inclined sidewall. These numbers were obtained both by calculations based on the center deflections and resonance frequency. When using these numbers together with Eq. A.1 the maximum difference between the deflection or resonance frequency calculated by FEM and the values obtained by assuming that the plate is clamped at the edge is reduced to 0.3% and 0.5% for structures b) and c), respectively.

Appendix B. Euler rotation

The rotation from the fixed crystal coordinate system, x_1–x_2–x_3, to the coordinate system of the plate, x_1'–x_2'–x_3', can be described using Euler angles. The rotation is performed by three consecutive rotations, as illustrated in Fig. B.12, which, using the so-called x-convention, are [26]
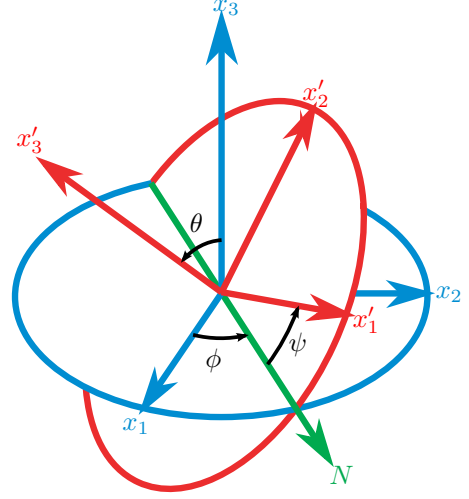
Figure B.12: Definition of the Euler rotation angles (ϕ, θ, ψ). The line of nodes, N, is the intersection of the x_1x_2 and the $x_1'x_2'$ coordinate planes.

1. Counterclockwise rotation of ϕ around the x_3–axis

$$\boldsymbol{a}_{\mathrm{I}}(\phi) = \begin{pmatrix} \cos\phi & \sin\phi & 0 \\ -\sin\phi & \cos\phi & 0 \\ 0 & 0 & 1 \end{pmatrix} \quad \text{(B.1)}$$

   moving x_1 to the line of nodes, N.

2. Counterclockwise rotation of θ around the line of nodes

$$\boldsymbol{a}_{\mathrm{II}}(\theta) = \begin{pmatrix} 1 & 0 & 0 \\ 0 & \cos\theta & \sin\theta \\ 0 & -\sin\theta & \cos\theta \end{pmatrix} \quad \text{(B.2)}$$

3. Counterclockwise rotation ψ around the x_3'–axis

$$\boldsymbol{a}_{\mathrm{III}}(\psi) = \begin{pmatrix} \cos\psi & \sin\psi & 0 \\ -\sin\psi & \cos\psi & 0 \\ 0 & 0 & 1 \end{pmatrix}. \quad \text{(B.3)}$$

The general rotation matrix, $\boldsymbol{a}$, is then the matrix product

$$\boldsymbol{a}(\phi, \theta, \psi) = \boldsymbol{a}_{\mathrm{III}}(\psi)\boldsymbol{a}_{\mathrm{II}}(\theta)\boldsymbol{a}_{\mathrm{I}}(\phi). \quad \text{(B.4)}$$

Appendix C. Coefficients

The coefficients $(\lambda_{00}^{\mathrm{o}}, \lambda_{11}^{\mathrm{o}}, \lambda_{20}^{\mathrm{o}}$ and $\lambda_{02}^{\mathrm{o}})$ in (47) are expressed in terms of the aspect ratio of the plate, $c = b/a$,

and the parameter F given by

$$
\begin{aligned}
F = &(18018000c^{16} + 4420c^{14}(-1331k_1^2 + 12560k_2) \\
&+ 18018000k_4^4 + 20c^{12}(-143(1825k_1^2k_2 - 12853k_2^2 \\
&+ 7266k_1k_3) + 30947760k_4) + 4420c^2k_4^2(-1331k_3^2 \\
&+ 12560k_2k_4) + c^6(-425711k_2^2k_3^2 + 88(84968k_2^3 \\
&- 119509k_1k_2k_3 - 885017k_3^2)k_4 + 20(-1082263k_1^2 \\
&+ 29959840k_2)k_4^2) + 20c^4k_4(-260975k_2k_3^2 \\
&+ 1837979k_2^2k_4 + 6k_4(-173173k_1k_3 + 5157960k_4)) \\
&- c^{10}(-7477184k_2^3 + 10516792k_1k_2k_3 + 21645260k_3^2 \\
&- 599196800k_2k_4 + 11k_1^2(38701k_2^2 + 7080136k_4)) \\
&+ 2c^8(163592k_2^4 + 33k_2^2(-9295k_1k_3 + 2338268k_4) \\
&+ 8k_4(-8891747k_1k_3 + 75117150k_4) \\
&- 4154150k_2(k_3^2 + k_1^2k_4))) \qquad (C.1)
\end{aligned}
$$

$$
\begin{aligned}
&\lambda_{00}^{\circ}F64a^4D_{\mathrm{a}}/p \\
&= 77(514800c^{12} + 130c^{10}(-979k_1^2 + 15058k_2) + 514800k_4^3 \\
&+ c^8(-57967k_1^2k_2 + 940446k_2^2 - 642044k_1k_3 + 26807760k_4) \\
&+ 130c^2k_4(-979k_3^2 + 15058k_2k_4) + c^4(-57967k_2k_3^2 \\
&+ 940446k_2^2k_4 + 4k_4(-160511k_1k_3 + 6701940k_4)) \\
&+ 2c^6(26026k_2^3 + k_2(-39039k_1k_3 + 8133028k_4) \\
&- 406315(k_3^2 + k_1^2k_4))) \qquad (C.2)
\end{aligned}
$$

$$
\begin{aligned}
&\lambda_{20}^{\circ}F128a^6D_{\mathrm{a}}/p \\
&= -1001(990c^{10}(3k_1^2 - 8k_2) \\
&- 514800k_4^3 + 1690c^2k_4(121k_3^2 - 412k_2k_4) \\
&- 2c^6(6292k_2^3 - 15301k_1k_2k_3 + 2079k_3^2 - 188097k_1^2k_4 \\
&+ 231012k_2k_4) + 5c^4(3575k_2k_3^2 - 48620k_2^2k_4 \\
&+ 12(9581k_1k_3 - 8904k_4)k_4) \\
&+ c^8(21879k_1^2k_2 - 7012k_1k_3 - 4(7403k_2^2 + 4860k_4))) \\
&\qquad (C.3)
\end{aligned}
$$

$$
\begin{aligned}
&\lambda_{02}^{\circ}F128a^6D_{\mathrm{a}}/p \\
&= 1001(514800c^{10} + 1690c^8(-121k_1^2 + 412k_2) \\
&+ 5c^6(-143(5(5k_1^2 - 68k_2)k_2 + 804k_1k_3) + 106848k_4) \\
&+ 990k_4(-3k_3^2 + 8k_2k_4) \\
&+ 2c^4(6292k_2^3 - 15301k_1k_2k_3 - 188097k_3^2 \\
&+ 2079k_1^2k_4 + 231012k_2k_4) + c^2(-21879k_2k_3^2 \\
&+ 29612k_2^2k_4 + 4k_4(1753k_1k_3 + 4860k_4))) \qquad (C.4)
\end{aligned}
$$

$$
\begin{aligned}
&\lambda_{11}^{\circ}F64a^6D_{\mathrm{a}}/p \\
&= 231(77220c^{10}k_1 + 260c^8(2011k_1k_2 - 847k_3) \\
&+ 77220k_3k_4^2 + 260c^2k_4(2011k_2k_3 - 847k_1k_4) \\
&+ c^6(143k_2(91k_1k_2 + 1892k_3) + 9621096k_1k_4) \\
&+ c^4(13013k_2^2k_3 + 270556k_1k_2k_4 + 9621096k_3k_4)). \quad (C.5)
\end{aligned}
$$

Appendix D. Young's modulus and Poisson's ratio for Si

For an anisotropic material exposed to a uniaxial stress $\boldsymbol{\sigma} = [\sigma_1, 0, 0, 0, 0, 0]^T$ one can define *directional* Young's modulus and Poisson's ratio as [18, 27, 38]

$$
E = 1/s_{11} \qquad (D.1)
$$
$$
\nu = -s_{21}/s_{11}. \qquad (D.2)
$$

For silicon we find

$$
1/E_{001} = s_{11}^{\mathrm{c}} + \frac{1}{4}\boldsymbol{\Delta}_s(-1 + \cos(4\psi)) \qquad (D.3)
$$
$$
1/E_{011} = s_{11}^{\mathrm{c}} + \frac{1}{16}\boldsymbol{\Delta}_s(-7 + 4\cos(2\psi) + 3\cos(4\psi)) \\
\qquad (D.4)
$$
$$
1/E_{111} = s_{11}^{\mathrm{c}} - \frac{1}{2}\boldsymbol{\Delta}_s \qquad (D.5)
$$
$$
= \frac{1}{2}s_{11}^{\mathrm{c}} + \frac{1}{2}s_{12}^{\mathrm{c}} + \frac{1}{4}s_{44}^{\mathrm{c}} \qquad (D.6)
$$

and

$$
\nu_{001} = \frac{\Delta_s(-1 + \cos(4\psi)) - 4s_{12}^{\mathrm{c}}}{\Delta_s(-1 + \cos(4\psi)) + 4s_{11}^{\mathrm{c}}} \qquad (D.7)
$$
$$
\nu_{011} = \frac{3\Delta_s(-1 + \cos(4\psi)) - 16s_{12}^{\mathrm{c}}}{\Delta_s(-7 + 4\cos(2\psi) + 3\cos(4\psi)) + 16s_{11}^{\mathrm{c}}} \qquad (D.8)
$$
$$
\nu_{111} = \frac{\Delta_s + 6s_{12}^{\mathrm{c}}}{3\Delta_s - 6s_{11}^{\mathrm{c}}} \qquad (D.9)
$$
$$
= \frac{s_{44}^{\mathrm{c}} - 2s_{11}^{\mathrm{c}} - 10s_{12}^{\mathrm{c}}}{3(2s_{11}^{\mathrm{c}} + 2s_{12}^{\mathrm{c}} + s_{44}^{\mathrm{c}})} \qquad (D.10)
$$

where the subscripts on E and ν denotes the orientation of the substrate. These expressions reproduce the figures shown in [18]. It is noted that the directional Young's modulus and Poisson ratio are constant for (111) silicon with the values $\nu_{111} = 0.262$ and $E_{111} = 169.0$ GPa, respectively.

Acknowledgments

[1] M. I. Haller, B. T. Khuri-Yakub, A surface micromachined electrostatic ultrasonic air transducer, IEEE Transactions on Ultrasonics Ferroelectrics and Frequency Control 43 (1) (1996) 1–6, ISSN 0885-3010, doi:10.1109/58.484456.

[2] O. N. Tufte, P. W. Chapman, D. Long, Silicon Diffused-Element Piezoresistive Diaphragms, Journal of Applied Physics 33 (11) (1962) 3322–3327, ISSN 00218979, doi:doi:10.1063/1.1931164.

[3] W. H. Ko, Q. Wang, Touch mode capacitive pressure sensors, Sensors and Actuators A-Physical 75 (3) (1999) 242–251, ISSN 0924-4247, doi:10.1016/S0924-4247(99)00069-2.

[4] G. Fragiacomo, K. Reck, L. Lorenzen, E. V. Thomsen, Novel Designs for Application Specific MEMS Pressure Sensors, Sensors 10 (11) (2010) 9541–9563, ISSN 1424-8220, doi: 10.3390/s101109541.

[5] K. Reck, E. V. Thomsen, O. Hansen, All-Optical Frequency Modulated High Pressure MEMS Sensor for Remote and Distributed Sensing, Sensors 11 (11) (2011) 10615–10623, ISSN 1424-8220, doi:10.3390/s111110615.

[6] S. Timoshenko, S. Woinowsky-Krieger, Theory of plates and shells, McGraw-Hill, 1959.

[7] R. Gregory, F. Wan, On plate theories and Saint-Venant's principle, International Journal of Solids and Structures 21 (10) (1985) 1005–1024, ISSN 00207683, doi:10.1016/0020-7683(85)90052-6.

[8] R. D. Gregory, F. Y. M. Wan, Boundary conditions at the edge of a thin or thick plate bonded to an elastic support, Journal of Elasticity 36 (2) (1994) 155–182, ISSN 0374-3535, doi: 10.1007/BF00040963.

[9] R. L. Taylor, S. Govindjee, Solution of clamped rectangular plate problems, Communications in Numerical Methods in Engineering 20 (10) (2004) 757–765, ISSN 1069-8299, doi: 10.1002/cnm.652.

[10] E. Ventsel, T. Krauthammer, Thin Plates & Shells: Theory, Analysis, & Applications, CRC Press, 1st edn., ISBN 0824705750, 2001.

[11] G. Kaminsky, Micromachining of silicon mechanical structures, Journal of Vacuum Science Technology B: Microelectronics and Nanometer Structures 3 (4) (1985) 1015 –1024, ISSN 1071-1023, doi:10.1116/1.583089.

[12] G. Kovacs, N. Maluf, K. Petersen, Bulk micromachining of silicon, Proceedings of the IEEE 86 (8) (1998) 1536 –1551, ISSN 0018-9219, doi:10.1109/5.704259.

[13] P. Rangsten, L. Smith, L. Rosengren, B. Hok, Electrostatically Excited Diaphragm Driven As A Loudspeaker, in: The 8th International Conference on Solid-State Sensors and Actuators, 1995 and Eurosensors IX.. Transducers '95, vol. 1, 430 –433, doi:10.1109/SENSOR.1995.717230, 1995.

[14] Q. Wang, W. H. Ko, Si-to-Si fusion bonded touch mode capacitive pressure sensors, Mechatronics 8 (5) (1998) 467–484, ISSN 0957-4158, doi:10.1016/S0957-4158(98)00013-0.

[15] Y. Huang, A. Ergun, E. Haeggstrom, M. Badi, B. Khuri-Yakub, Fabricating capacitive micromachined ultrasonic transducers with wafer-bonding technology, Journal of Microelectromechanical Systems 12 (2) (2003) 128 – 137, ISSN 1057-7157, doi: 10.1109/JMEMS.2003.809968.

[16] G. Fragiacomo, T. Pedersen, O. Hansen, E. V. Thomsen, Intrinsic Low Hysteresis Touch Mode Capacitive Pressure Sensor, in: 2010 IEEE Sensors, IEEE, New York, ISBN 978-1-4244-8168-2, 2279–2282, WOS:000287982100504, 2010.

[17] K. E. Petersen, Silicon as a mechanical material, Proceedings of the IEEE 70 (5) (1982) 420–457, ISSN 00189219, 15582256.

[18] J. J. Wortman, R. A. Evans, Young's Modulus, Shear Modulus, and Poisson's Ratio in Silicon and Germanium, Journal of Applied Physics 36 (1) (1965) 153, ISSN 00218979, doi: 10.1063/1.1713863.

[19] S. D. Senturia, Microsystem design, Kluwer Academic Publishers, Boston, ISBN 0792372468 9780792372462, 2001.

[20] J. A. Pelesko, D. H. Bernstein, Modeling MEMS and NEMS, Chapman & Hall/CRC, Boca Raton, FL, ISBN 1584883065 9781584883067, 2003.

[21] V. Kaajakari, Practical MEMS, Small Gear Pub., Las Vegas, Nev., ISBN 0982299109 9780982299104, 2009.

[22] J. Korvink, O. Paul, MEMS: A Practical Guide of Design, Analysis, and Applications, Springer, ISBN 9783540211174, 2006.

[23] W. K. Schomburg, Introduction to Microsystem Design, Springer-Verlag, Berlin, ISBN 3642194885; 9783642194887., 2011.

[24] S. Holgate, The Transverse Flexure of Perforated Aeolotropic Plates, Proceedings of the Royal Society of London Series A-Mathematical and Physical Sciences 185 (1000) (1946) 50–69, doi:10.1098/rspa.1946.0004.

[25] C. Hwu, Anisotropic Elastic Plates, Springer, ISBN 9781441959157, 2010.

[26] R. E. Newnham, Properties of Materials: Anisotropy, Symmetry, Structure, Oxford University Press, USA, ISBN 019852076X, 2005.

[27] J. F. Nye, Physical Properties of Crystals: Their Representation by Tensors and Matrices, Oxford University Press, USA, ISBN 0198511655, 1985.

[28] L. L. D. Landau, E. M. Lifshitz, A. M. Kosevich, L. P. Pitaevskii, Course of Theoretical Physics: Theory of elasticity, Elsevier, ISBN 9780750626330, 1986.

[29] T. C. T. Ting, Anisotropic Elasticity: Theory and Applications, Oxford University Press, USA, ISBN 0195074475, 1996.

[30] A. E. H. Love, A Treatise on the Mathematical Theory of Elasticity, Dover Publications, 4 edn., 1944.

[31] E. Illing, The Bending of Thin Anisotropic Plates, The Quarterly Journal of Mechanics and Applied Mathematics 5 (1) (1952) 12–28, ISSN 0033-5614, 1464-3855, doi: 10.1093/qjmam/5.1.12.

[32] I. Ladabaum, X. C. Jin, H. T. Soh, A. Atalar, B. T. Khuri-Yakub, Surface micromachined capacitive ultrasonic transducers, IEEE Transactions on Ultrasonics Ferroelectrics and Frequency Control 45 (3) (1998) 678–690, ISSN 0885-3010, doi: 10.1109/58.677612.

[33] M. la Cour, T. Christiansen, J. Jensen, E. V. Thomsen, Modeling of CMUTs with Anisotropic Plates, IEEE, 2012.

[34] F. C. Mbakogu, M. N. Pavlovic, Bending of clamped orthotropic rectangular plates: a variational symbolic solution, Computers & Structures 77 (2) (2000) 117–128, ISSN 0045-7949, doi: 10.1016/S0045-7949(99)00217-5.

[35] J. Hall, Electronic Effects in the Elastic Constants of n-Type Silicon, Physical Review 161 (3) (1967) 756–761, ISSN 0031-899X, 1536-6065, doi:10.1103/PhysRev.161.756.

[36] F01 Committee, Practice for Conversion Between Resistivity and Dopant Density for Boron-Doped, Phosphorus-Doped, and Arsenic-Doped Silicon, Tech. Rep., ASTM International, URL http://www.astm.org/Standards/F723.htm, 1999.

[37] M. la Cour, T. Christiansen, C. Dahl-Petersen, K. Reck, O. Hansen, J. Jensen, E. V. Thomsen, Modeling and Measurements of CMUTs with Square Anisotropic Plates, IEEE, 2013.

[38] J. Turley, G. Sines, The anisotropy of Young's modulus, shear modulus and Poisson's ratio in cubic materials, Journal of Physics D: Applied Physics 4 (2) (1971) 264–271, ISSN 00223727, doi:10.1088/0022-3727/4/2/312.